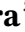


## RESEARCH ARTICLE

# Long-term snowfall trends and variability in the Alps

Michele Bozzoli<sup>1,2</sup>  | Alice Crespi<sup>3</sup>  | Michael Matiu<sup>1</sup>  | Bruno Majone<sup>1</sup>  |  
Lorenzo Giovannini<sup>1</sup>  | Dino Zardi<sup>1,4</sup>  | Yuri Brugnara<sup>5</sup>  |  
Alessio Bozzo<sup>6</sup>  | Daniele Cat Berro<sup>7</sup> | Luca Mercalli<sup>7</sup> | Giacomo Bertoldi<sup>2,3</sup> 

<sup>1</sup>Department of Civil, Environmental and Mechanical Engineering, University of Trento, Trento, Italy

<sup>2</sup>Institute for Alpine Environment, Eurac Research, Bolzano, Italy

<sup>3</sup>Center for Climate Change and Transformation, Eurac Research, Bolzano, Italy

<sup>4</sup>Center for Agriculture, Food and Environment, University of Trento, Trento, Italy

<sup>5</sup>Laboratory for Air Pollution/Environmental Technology, Dübendorf, Switzerland

<sup>6</sup>European Organisation for the Exploitation of Meteorological Satellites—EUMETSAT, Darmstadt, Germany

<sup>7</sup>Italian Meteorological Society, Torino, Italy

**Correspondence**

Michele Bozzoli, Department of Civil, Environmental and Mechanical Engineering, University of Trento, Trento, Italy.

Email: michele.bozzoli@unitn.it

**Funding information**

Università degli Studi di Trento; Eurac Research, Grant/Award Number: D55F21005230003; Swiss National Science Foundation (SNSF); Autonomous Province of Bolzano (Italy)

**Abstract**

Snow is particularly impacted by climate change and therefore there is an urgent need to understand the temporal and spatial variability of depth of snowfall (HN) trends. However, the analysis of historical HN observations on large-scale areas is often impeded by lack of continuous long-term time series availability. This study investigates HN trends using observed time series spanning the period 1920–2020 from 46 sites in the Alps at different elevations. To discern patterns and variations in HN over the years, our analysis focuses also on key parameters such as precipitation (P), mean air temperature (TMEAN), and large-scale synoptic descriptors, that is, the North Atlantic Oscillation (NAO), Arctic Oscillation (AO) and Atlantic Multidecadal Oscillation (AMO) indices. Our findings reveal that in the last 100 years and below 2000 m a.s.l., despite a slight increase in winter precipitation, there was a decrease in HN over the Alps, especially for southern and low-elevation sites. The South-West and South-East regions experienced an average loss of 4.9 and 3.8%/decade, respectively. A smaller relative loss was found in the Northern region (2.3%/decade). The negative HN trends can be mainly explained by an increase of TMEAN by 0.15°C/decade. Most of the decrease in HN occurred mainly between 1980 and 2020, as a result of a more pronounced increase in TMEAN. This is also confirmed by the change of the running correlation between HN and TMEAN, NAO, AO over time, which until 1980 were not correlated at all, while the correlation increased in later years. This suggests that in more recent years favourable combinations of temperature, precipitation, and atmospheric pattern have become more crucial for snowfall to occur. On the other hand, no correlation was found with the AMO index.

**KEYWORDS**

Alps, correlation, depth of snowfall, trends, variability

This is an open access article under the terms of the Creative Commons Attribution License, which permits use, distribution and reproduction in any medium, provided the original work is properly cited.

© 2024 The Authors. *International Journal of Climatology* published by John Wiley & Sons Ltd on behalf of Royal Meteorological Society.

## 1 | INTRODUCTION

Snow plays a critical role in our planet and its ecosystems, influencing many environmental processes. Snow acts as a freshwater reservoir, storing a substantial portion of the annual precipitation on the Earth (Aragon & Hill, 2024; Isotta et al., 2014). This stored water gradually melts during warmer months, supporting river flows and groundwater recharge in mountain and downstream areas (Qi et al., 2020). Furthermore, the reflective properties of snow affect the planet's energy balance, influencing radiative forcing and regional climate patterns (Perovich, 2007; Zhuravleva & Kokhanovsky, 2011). Surface-layer turbulence, land-atmosphere exchanges and transport processes in the atmospheric boundary layer are strongly modified over snow-covered terrain (Tomasi et al., 2017). Finally, the presence and availability of snow are the fundamental prerequisites for many recreational activities, and therefore a key factor for winter mountain tourism (Beniston, 2012; Olefs et al., 2020; Rixen et al., 2011).

It is well known that climate change also affects snow dynamics. The consequences of warming temperatures on snow cover and associated environmental systems are underscored by a wealth of scientific literature. Carrer et al. (2023), Mote et al. (2018), Olefs et al. (2017), and Valt and Cianfarra (2010) show the observed decrease in snow cover and duration in various regions due to increasing temperatures. This phenomenon, highlighted as a key indicator of climate change by the Intergovernmental Panel on Climate Change (IPCC), is modifying the hydrological cycle and will affect the availability of water resources (Bavay et al., 2009; Milner et al., 2017).

The necessity of establishing and maintaining long-term snow observations is strongly recommended, as these records play a crucial role in understanding the interplay between snow dynamics, climate change, and associated environmental impacts. In addition, it helps to provide indications for adaptation to changing snow regimes, water resources management, and the improvement of climate models. Leporati and Mercalli (1994) highlight the importance of continuous snow observations to assess trends in the extent, duration and properties of snow cover over long periods. Brown and Mote (2009) believe that long snow cover datasets are essential for improving our understanding of the response of the northern hemisphere snow cover to climate change, and for projecting potential shifts in water availability (Barnett et al., 2008). However, maintaining comprehensive and consistent long-term snow observations faces several challenges, including instrument reliability, funding stability, and data harmonization (Marcolini et al., 2017, 2019). Moreover, the analysis of long-term

time series requires dealing with artificial inhomogeneities introduced by station relocations and changes in the measurement procedure (Buchmann et al., 2022; Resch et al., 2023).

Numerous studies on long-term trends of snow in the Alps have yielded valuable information about the impacts of climate change in this region. Durand et al. (2009) and Marty (2008) documented a consistent trend of declining snow cover duration (SCD) and snow depth (HS) over decades. According to Marty et al. (2017, 2023) the snow water equivalent (SWE) showed a significant decrease during the last six decades in the European Alps, more pronounced during spring than during winter, with the snow becoming wetter and more variable. Those results were also confirmed for the Italian Alps by Colombo et al. (2022). Decreasing trends of HS were observed for the entire Alpine region by Matiu et al. (2021). They evaluated linear trends of mean monthly HS between 1971 and 2019. The study concluded that 87% of the stations analysed were characterized by a decrease, with stronger negative trends from March to May than from December to February. An overall declining trend showing a reduction ranging from 11 to 15 days was found by Marke et al. (2018), where SCD was compared among various sub-regions of Austria for the time intervals 1950–1979 and 1980–2009. Laternser and Schneebeli (2003) conducted a study in the Swiss Alps, noting that the average HS and SCD showed similar patterns from 1931 to 1999: an initial general increase until the 1980s was followed by a statistically significant decrease toward the end of the century. These findings were also confirmed by Serquet et al. (2011), who examined seasonal trends and the temperature-dependent relationship between snowfall and precipitation days in Switzerland from 1961 to 2008.

The interplay between snow and various climatic factors, including precipitation, temperatures, and teleconnection indices, represents a complex interaction, and significantly influences snow dynamics with implications for regional climates. In the Trentino-South Tyrol region (south-eastern Alps), Bertoldi et al. (2023) found that precipitation patterns directly influence snowfall accumulation and subsequently shape snow cover extent and depth. Temperature changes, as discussed by Beniston et al. (2018) and Serquet et al. (2011), can alter the phase of precipitation from snow to rain, impacting snowpack persistence and seasonal patterns. Teleconnection indices, such as the North Atlantic Oscillation (NAO) and the Arctic Oscillation (AO), play a role in modulating large-scale atmospheric circulation patterns that influence regional climate and precipitation, as shown by Hurrell et al. (2003). For example, on a European level, Bartolini et al. (2010) noted a connection between snow cover and large-scale atmospheric patterns over the period 1972–

2006, specifically highlighting a robust correlation with AO during the winter months. Another important index is the Atlantic Multidecadal Oscillation (AMO), which varies on multi-decadal timescales, alternating warm and cool phases that can last for several decades each (Abiy et al., 2019). AMO can influence various aspects of climate, including patterns of temperature and precipitation, which can, in turn, impact snowfall in different regions (Hunter et al., 2006).

It was decided to choose depth of snowfall (HN) because it is the variable that best represents the total winter solid precipitation. It is important to recover HN observations, understand their change over time, and compare them with liquid precipitation trends, as HN and the solid–liquid precipitation ratio are very sensitive to climate change (Bertoldi et al., 2023; Guo & Li, 2015). HN, being solid precipitation, is easier to compare with liquid precipitation than HS. This comparison is essential for understanding the relative influence of snowfall and liquid precipitation on climate trends. Additionally, the seasonal HN is crucial for assessing the suitability of winter sports activities (Morin et al., 2021). While SWE is more meaningful hydrologically, long-term data for it are scarce. Historical records, particularly at low elevations, often focus on HN rather than HS or SWE, making this study an opportunity to highlight and utilize these historical time series.

Efforts to analyse historical HN observations on large-scale areas are often impeded by the challenges of retrieving and harmonizing long, continuous observed time series across extensive geographical areas. Thus, the main novelty of this study is the investigation and analysis of long-term series of HN observations that cover at least 100 years from 1920 to 2020. In addition to the length of the series, another relevant novelty compared to previous studies is the coverage of the whole Alpine domain using 46 sites located at different elevations (from 57 m up to 1878 m a.s.l.), whereas previous studies on HN often focused on the northern or southern part of the Alps. Therefore, the objectives of this study are to evaluate how HN has changed in the past century and to analyse the spatial variability of trends. Furthermore, in order to identify the drivers behind these changes, we test correlations between HN and precipitation (P), mean air temperature (TMEAN) and large-scale synoptic descriptors, that is, NAO, AO and AMO indices, and assess if and how these correlations have changed over time. From here on we will refer to depth of snowfall as simply snowfall.

The article is structured as follows: Sections 2 and 3 describe the observation database and the techniques used to derive statistics and trends. Section 4 provides results on trends, and Section 5 discusses them. Finally,

Section 6 summarizes the results and draws some conclusions.

## 2 | DATA

### 2.1 | Study area

The study area of this study is an extended region of the Alpine domain, similar to the “Greater Alpine Region” defined by Auer et al. (2007). Stretching over a distance of more than 1000 km, the Alps form an arc-shaped structure that spans from the Mediterranean coasts of France and Italy to the Lowlands east of Vienna. They cover southeastern France, Switzerland, northern Italy, southern Germany, Austria, and Slovenia (Figure 1). The Alpine region displays intricate topography, marked by substantial elevation shifts and deep valleys oriented in various directions, intersecting the main ridge and forming numerous mountain massifs.

In terms of climate, the Alps occupy a transition zone where three major climatic influences converge. The Atlantic Ocean region, characterized by a moderately humid climate, the Mediterranean Sea region, marked by dry summers and mild, wet winters, and the European continental area with cold, dry winters and warm summers (Auer et al., 2005; Monteiro & Morin, 2023). In addition to these three climatic zones, local effects related to elevation and the complex Alpine terrain must also be considered. As a consequence, the interplay of these three climatic zones, combined with the Alps topography, gives rise to climatic gradients along both the north–south and west–east axes.

### 2.2 | Snowfall data

The HN database used in this study is composed of 70 stations located in the Alpine region (Figure 1). The list of all the stations used and their relative metadata can be found in Table A1. However, only 46 of them are used for trend analysis, as the remaining time series are very fragmented with many missing data, allowing them to be used only for the homogenization procedure (see Section 3 for details on data homogenization). The highest number of stations and data starts from the early 1900s (Figure 2). Moreover, the number of available stations has decreased in the most recent years, since not all of the series were kept regularly up to date. For this reason, the period 1920–2020 was chosen for the analysis.

Data were kindly provided by several organizations, such as GeoSphere Austria (GSA), Swiss Federal Office of Meteorology and Climatology (METEOSWISS),

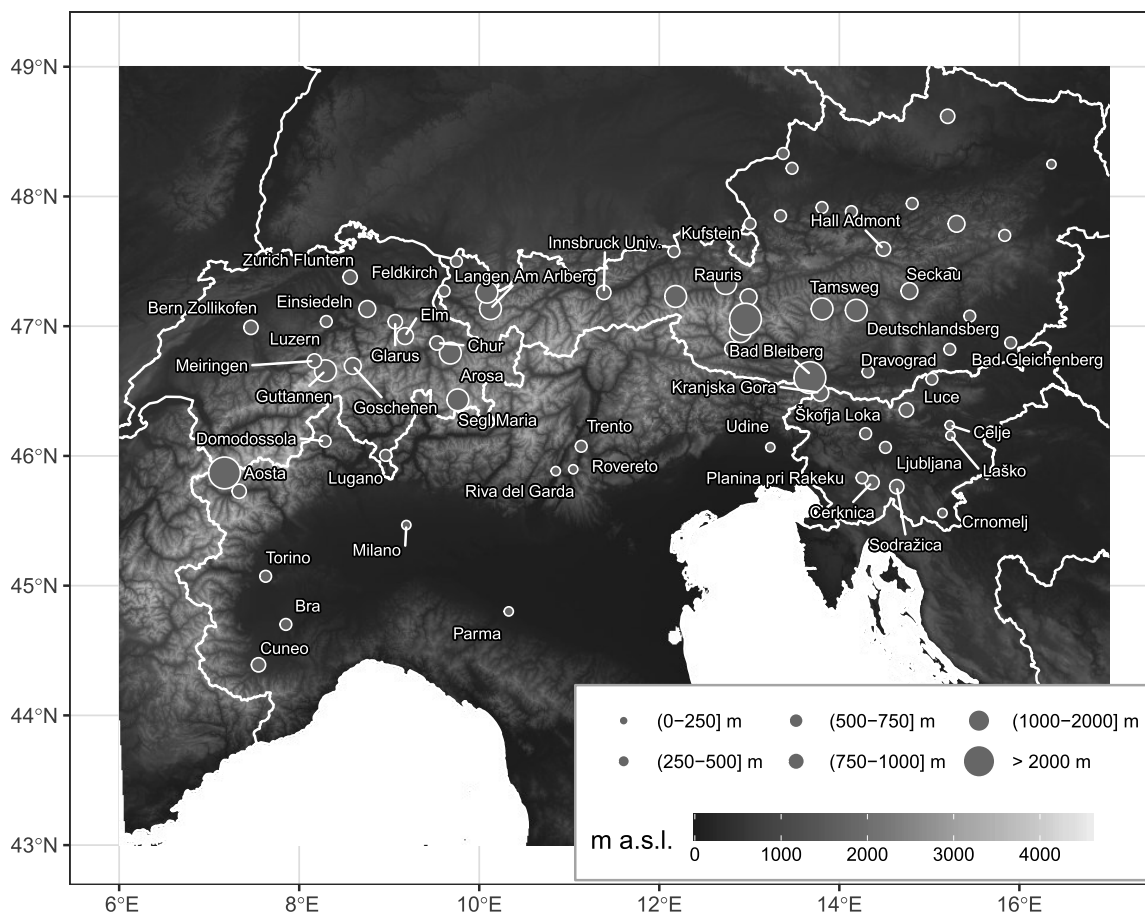


**FIGURE 1** Location of the snowfall (HN) stations in the Alps. Labelled dots indicate stations used for trend analysis. The size of the dots is proportional to the site elevation.

Slovenian Environment Agency (ARSO), Società Meteorologica Italiana (SMI), Meteotrentino (MTN), Meteotrentino Alto Adige (MTAA), Società Meteorologica Alpino-Adriatica (SMA-A), Fondazione Osservatorio Meteorologico Milano Duomo (OMD) and Osservatorio Meteorologico di Parma (OMP).

HN data are taken daily. The largest part of the data comes from manual measurements. As suggested by Matiu et al. (2021), while the observers follow slightly different guidelines in each country or network, the observation modalities are remarkably similar, thus allowing a combination of the different sources. A daily measurement of HN is taken using a ruler and measuring the height of fresh snow that had fallen in the previous 24 h over a wooden table in the early morning hours, generally between 07.00 and 09.00 LST (UTC + 1). For more detailed information on the measuring modalities, we refer to the European Snow Booklet (Haberkorn, 2019). Data were provided as monthly sums, except for data from Slovenia, which were provided with daily frequency. We then aggregated the monthly values into seasonal sums considering the months from November to

May. This definition of the snow season was chosen in order to maximize the availability of HN data in the study region and cover both winter and spring.

### 2.3 | Meteorological data and teleconnection indices

We analyse long-term homogenized weather data in the Alps in order to compare HN to meteorological data. For TMEAN, we use the Historical Instrumental climatological Surface Time series of the greater ALPine region (HISTALP, Auer et al., 2007) (version Grid-mode-2). The Grid-mode-2 dataset includes values of monthly mean air temperature distributed on a regular grid with a resolution of 5', ranging from 4° to 19° E and from 43° to 46° N, covering the period 1780–2014. For P, we use the Long-term Alpine Precipitation reconstruction dataset (LAPrec, Isotta et al., 2024) (version LAPrec1901.v1.1), which combines the high-resolution spatial information from the Alpine Precipitation Grid Dataset (APGD) with homogenized temporal information from HISTALP

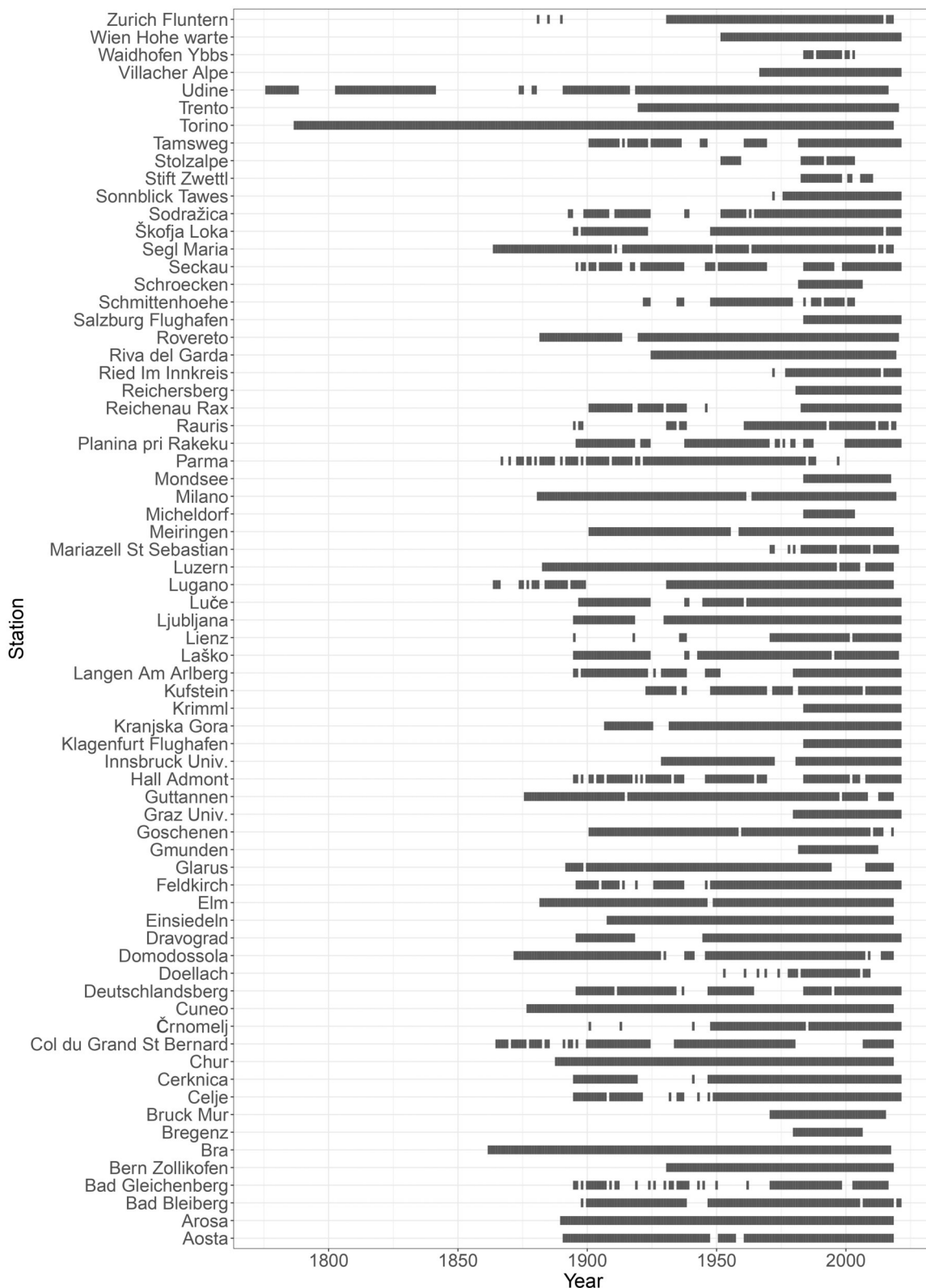


**FIGURE 2** Seasonal snowfall (HN) data availability for each station per year. Grey bars indicate that data are present; white spaces indicate no data available.

precipitation series. The LAPrec1901.v1.1 version is a gridded dataset that includes monthly precipitation sums from 1 January 1901 to 31 December 2019 with a grid

spacing of 5 km covering the Alpine region (approx. from 43–49° N to 4–17° E, land area only). TMEAN and P time series at each station location were extracted from the

gridded datasets by considering the nearest neighbouring grid cell. For the TMEAN data, as suggested by Rolland (2003), we applied a correction for the elevation mismatch between the HISTALP grid and the stations, considering a lapse rate correction of  $0.5^{\circ}\text{C}/100\text{ m}$ . Both TMEAN and P dataset end a few years earlier compared to the considered HN time series. However, adding more recent observations from other sources could introduce inhomogeneities that can affect the analyses, so we limit the comparison of HN to weather data to 2014. For teleconnection indices, series of NAO, AO, and AMO are obtained from the National Oceanic and Atmospheric Administration (NOAA) website (<https://psl.noaa.gov/data/climateindices/list>), with data starting in 1950. In the end, all those data are aggregated to seasonal scale, that is, from November to May.

### 3 | METHODS

#### 3.1 | Quality check, homogenization and gap filling

Quality control procedures are crucial for identifying anomalies or deviations in HN data series (Baronetti et al., 2019). As suggested by Diodato et al. (2020), in order to study long-term HN regime changes and assess climate anomalies, the homogeneity of HN time series has to be investigated to identify breakpoints and the impact of the possible corrections.

In this study, we use the Climatol procedure, as implemented in the R package “climatol” version 3.1.1 (Guijarro, 2018) to check the homogeneity of the HN time series. Climatol evaluates the homogeneity using the Standard Normal Homogenization Test (SNHT, Alexandersson & Moberg, 1997) (see below for details in Appendix B). Since Climatol revealed that all the time series were sufficiently homogeneous, we did not apply any specific corrections. However, considering the monthly HN distribution of each station, 24 stations resulted not suitable for the trend analysis due to the presence of frequent missing data and a total of 46 stations are those selected for the trend analysis (see “Use” = HT in Table A1).

To fill in the gaps of the monthly HN series, we follow the procedure proposed by Bertoldi et al. (2023) and Matiu et al. (2021). This procedure is able to reconstruct monthly values of a station (test station) through a weighted average of the records available from up to 10 neighbouring stations (reference stations). The reference stations are selected using a proximity criterion considering weights depending on horizontal and vertical distances. The weights are evaluated using an

exponential decay (“half-time” transformation of the decay constant). In our case, we found the best reconstruction accuracy setting 50 km and 250 m for the horizontal and vertical distance halving coefficients for station weights, respectively, and 10 as the minimum number of years with common data between test and reference series. Considering only the months analysed, 12.1% of the total monthly data were missing. After the gap filling reconstruction, all the data are aggregated into seasonal sums.

#### 3.2 | Statistical analyses

Long-term trends in HN data are detected with a series of statistical tests. With the Mann-Kendall (MK) trend test (Kendall, 1975; Mann, 1945) we assess the significance of trends over time. The MK test detects monotonic upward or downward trends, indicating consistent increases or decreases in the variable over time, regardless of whether or not the trend is linear. In this study, statistical significance is indicated by a  $p$  value  $<0.05$  unless otherwise specified. The trend magnitudes are assessed with the non-parametric method developed by Sen (1968). This approach estimates the linear trend slope in the sample of all  $N$  data pairs. The median value of all the slopes calculated for each data pair reflects the overall steepness of the trend.

Finally, to assess the bivariate relationship between time series of variables (HN vs. P, TMEAN, NAO, AO, and AMO), we use the Spearman correlation coefficient  $\rho$ . The parameter  $\rho$  tends toward either +1 or -1 when the monotonic association between the two variables is stronger, with negative numbers describing anti-correlation. A value close to 0 denotes the absence of any association between the two variables.

#### 3.3 | Regionalization

We identify groups of similar stations with an automated clustering procedure based on k-means of monthly HN series without including any location information. Based on the elbow method and silhouette metrics, three clusters are identified as optimal (see Appendix C and Figure A4). The resulting clusters are named South-East (SE), South-West (SW), and North (N). The SE cluster counts 16 stations that range from 113 m to 909 m a.s.l. with a mean elevation of 442 m a.s.l. It includes all Slovenian stations, some Austrian stations (Bad Bleiberg, Deutschlandsberg, Bad Gleichenberg, Seckau) and Udine in north-eastern Italy. Here, HN is favoured by the advection of cold air from

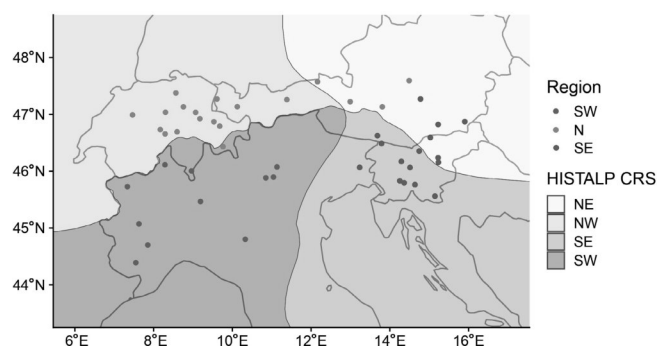


**FIGURE 3** Clustering of stations based on seasonal snowfall (HN) data. Three regions are detected: South-West (SW) (blue dots), North (N) (green dots) and South-East (SE) (red dots). Underlaid are the HISTALP coarse-resolution subregions (Auer et al., 2007).

northern or northeastern Europe, which then interacts with the wetter and warmer air of the Mediterranean Sea. The SW cluster has 11 stations ranging from 57 to 565 m a.s.l., with a mean elevation of 272 m a.s.l. It covers almost the entire southern side of the Italian Alpine region, including some stations in the Po Valley (e.g., Torino, Milano, Parma) and others in the Alpine valleys (e.g., Aosta, Domodossola, Trento). In this region, snow is mainly caused by the advection of warm and humid air from the south flowing over pre-existing cold air. The N cluster counts 19 stations going from 438 m to 1878 m a.s.l., with a mean elevation of 850 m a.s.l. and includes all Swiss stations and the Austrian stations that are not included in the SE cluster. HN is mainly caused by the descent of cold air masses from northern Europe, which, colliding with the Alpine chain, can lead to cold temperatures and heavy precipitation.

These three clusters are compared with the regionalization obtained from the HISTALP project (Auer et al., 2007) in Figure 3. There is an overall agreement between the clusters identified from HN series and the climate regions of HISTALP, which are based on a combination of air temperature, precipitation, air pressure, sunshine, and cloudiness. The mismatch in the northern and eastern parts of the Alpine region is likely due to the fact that the largest contribution to the HISTALP region definition comes from air temperature, while the division based on HN is more driven by the precipitation regime. Finally, it is worth noting that the HN regions are qualitatively similar to the clusters based on snow depth (HS) identified by Matiu et al. (2021).

All computations are performed with the statistical software R (version 4.2.2), using the RStudio interface version 1.1.494 (R Core Team, 2020).

## 4 | RESULTS

### 4.1 | Climatology

HN, P and TMEAN climatology for all the stations analysed is shown in Figure 4. Data are divided following the three reference areas discussed in the previous section and refer to all the months included in the snow season, that is, November to May, from the 1920–1921 to the 2019–2020 season.

As can be seen in Figure 4a, HN values increase with elevation, with the highest stations recording the highest seasonal accumulations. However, this increase is not entirely linear. It remains so up to around 700 m a.s.l. and then the signal starts becoming more noisy, also due to the low number of stations at high elevations. The maximum value of the average seasonal HN accumulation is at Langen Am Arlberg (1270 m a.s.l.) with 829 cm, followed by Arosa (1878 m a.s.l.) and Guttannen (1055 m a.s.l.) with 663 and 516 cm, respectively. Note that all these stations are located in the N region, where stations are on average at higher elevations than in the others. In the SE and SW regions the average seasonal HN accumulation is much lower, with a maximum of 250 cm at Kranjska Gora (802 m a.s.l.) and 111 cm at Cuneo (565 m a.s.l.). However, the comparison of HN totals at locations at the same elevation in the SW and SE regions shows that the latter records more snow than the former, indicating that the SE region is more snowy than the SW region.

The distribution of seasonal P climatology is very irregular (Figure 4b), without a clear correlation with elevation. No differences in P climatology among the regions are evident and the distribution with elevation exhibits a strong variability among the sites, since orography affects P at a much smaller spatial scale in such a complex area as the Alpine chain. However, this can be reasonable if we think that here we are considering averages made with 100 years of cumulative seasonal P data, that is, from November to May. Therefore, it is plausible that the orographic pattern of P with elevation tends to be smoother. On average, in the SW region the seasonal P accumulation is 554 mm, slightly less than the 673 mm of the SE region and the 639 mm of the N region. However, from Figure 4b it is clear that P is very variable in all the three regions, so these average values are not representative of the P climatology of the single stations. Guttannen (1055 m a.s.l.) in the N region and Planina pri Rakeku (462 m a.s.l.) in the SE region are the two stations with the highest values of seasonal P accumulation: 966 and 962 mm, respectively.

The seasonal TMEAN climatology, as expected, is highly correlated with elevation: the warmest value is

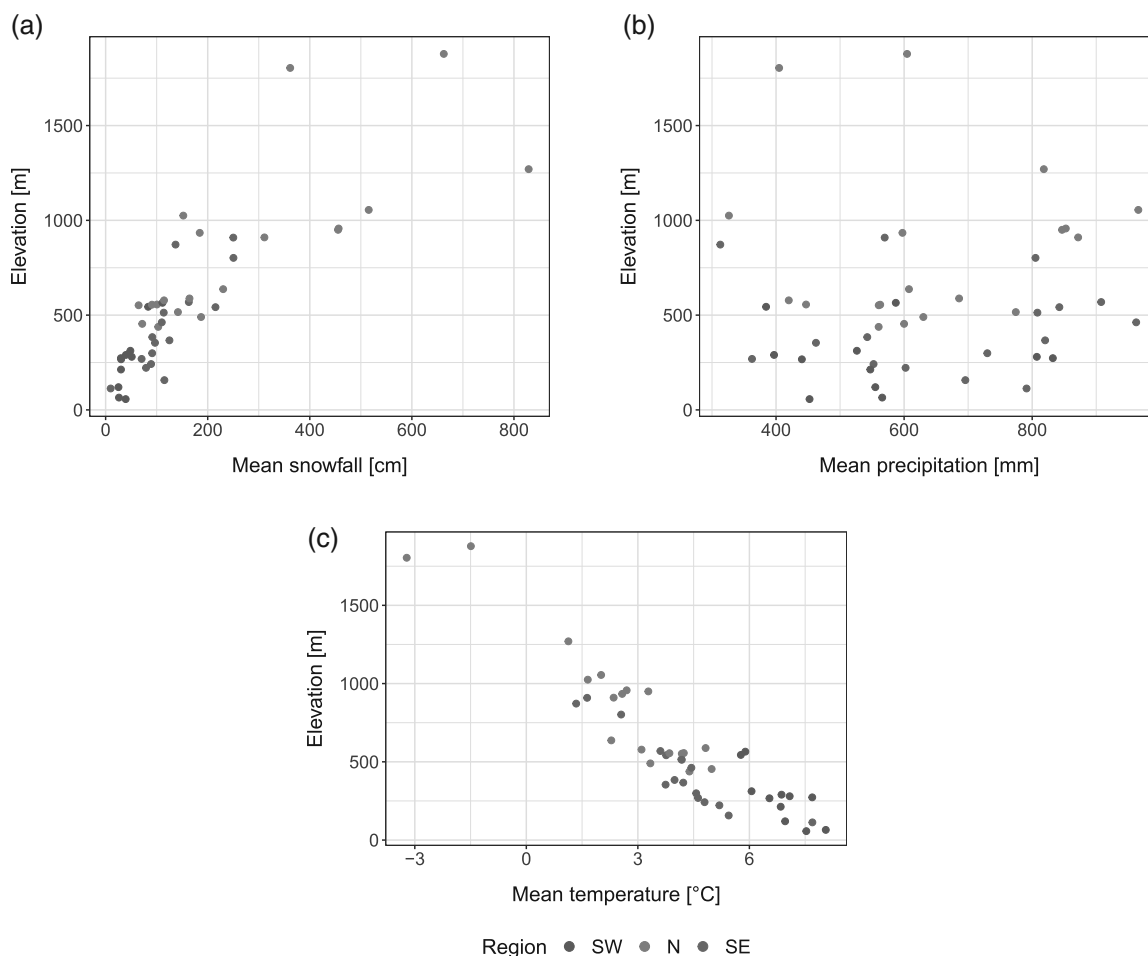


**FIGURE 4** Elevation distribution of seasonal snowfall (HN) (a), precipitation (P) (b) and mean air temperature (TMEAN) (c) climatology grouped by region.

+8.1°C at Riva del Garda (65 m a.s.l.) and the coldest one is  $-3.2^{\circ}\text{C}$  at Segl Maria (1804 m a.s.l.). It is interesting to notice that, while at the same elevation the stations in the N and SE regions have comparable values, the locations in the SW region are warmer. On average, the seasonal TMEANs for N, SE and SW stations are  $+2.7^{\circ}\text{C}$ ,  $+4.1^{\circ}\text{C}$  and  $+6.9^{\circ}\text{C}$ , respectively.

## 4.2 | Trend analysis

This section presents the results of the trend analysis and how trends change with elevation. As shown in Figure 5, over the last 100 years, most stations record a negative HN trend. On average, the trend is of  $-3.4\%$ /decade. The only three stations that show a positive trend are Hall Admont (637 m a.s.l.), Arosa (1878 m a.s.l.), and Kufstein (490 m a.s.l.), all in the N region, with  $+0.9$ ,  $+0.5$  and  $+0.4\%$ /decade, respectively. However, none of them turn out to be statistically significant. HN trends are highly elevation-dependent (Figure 6). The

stations in the SW region and thus those at lower elevations, are experiencing the greatest losses in terms of HN, with all stations showing negative trends and 54.5% of them also statistically significant. Instead, the dependence on altitude is less pronounced for the SE region. However, also in this case the majority (87.5%) of the trends are negative and statistically significant. Note that, at the same elevation, stations in the SE region have less negative trends than those in the SW region. For the N region, again the dependence on elevation is very strong. Stations at lower elevations show negative and significant trends, while trends are less negative for higher stations.

P trends show a different behaviour depending on the region. There is a clear prevalence of increasing trends in the SW and N regions, with average values of  $+0.3$  and  $+0.8\%$ /decade, respectively. However, only two cases in the N region are statistically significant: Luzern (454 m a.s.l.) with  $+1.3\%$ /decade and Zurich Fluntern (555 m a.s.l.) with  $+1.6\%$ /decade, which represents the highest P trend of the dataset. Instead, in the SE region,



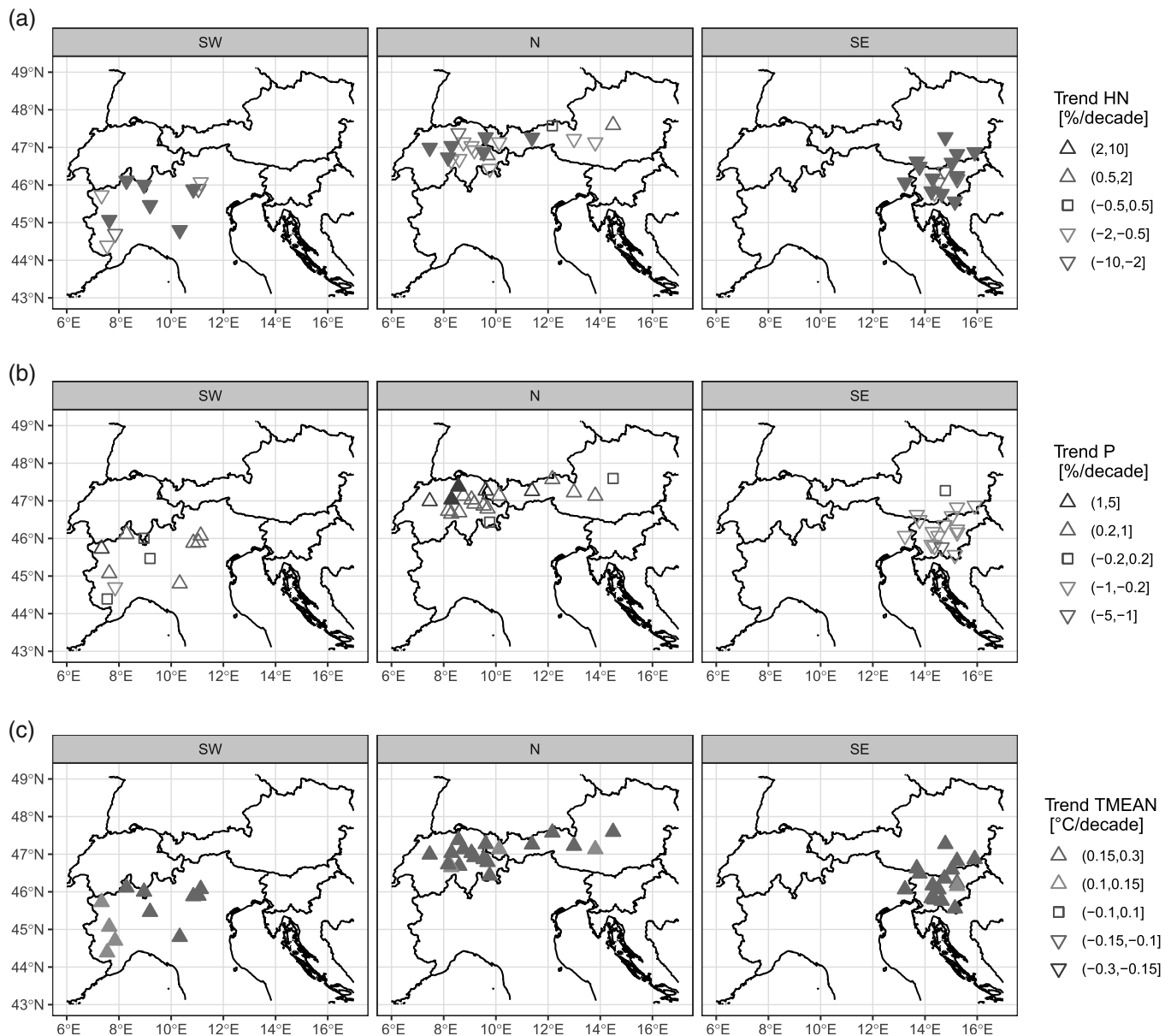


**FIGURE 5** Spatial distribution of seasonal snowfall (HN) (a), precipitation (P) (b) and mean air temperature (TMEAN) (c) trends expressed in [%/decade], [%/decade], and [°C/decade], respectively. Each point represents one station and the corresponding trend value: Blue (red) triangles indicate positive (negative) trends; grey squares indicate negligible trends. Full symbols indicate significant trends.

trends are all negative, with an average of  $-0.7\%/decade$  and a minimum of  $-1.1\%/decade$  at Sodrazica (542 m a.s.l.). However, none of them is statistically significant. In contrast to HN trends, there is no dependency on elevation (Figure 6).

In all the three regions, TMEAN trends are all positive and statistically significant. On average, the SW, N and SE regions present very similar trends:  $+0.15$ ,  $+0.16$ , and  $+0.16\text{°C}/decade$ , respectively. Also the variability between the single stations is rather low, with no dependence on elevation. The maximum positive trend is at Zurich Fluntern (555 m a.s.l.) in the N region with

$+0.18\text{°C}/decade$ , while Bra (290 m a.s.l.) in the SW region shows the lowest warming, with  $+0.13\text{°C}/decade$ .

### 4.3 | Trend temporal variability

Besides considering the overall trend, it is interesting to analyse how HN, P, and TMEAN change over time. To this purpose, we consider here 21-year moving average anomalies of seasonal HN, P, and TMEAN. HN and P anomalies are calculated by dividing every time series by its mean and then multiplying them by 100 to get %

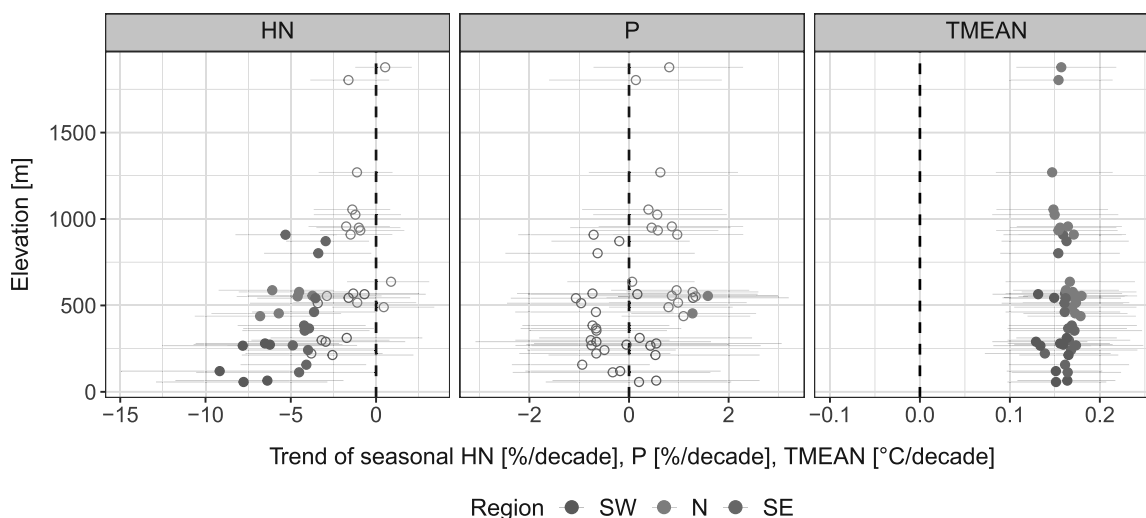


**FIGURE 6** Seasonal snowfall (HN), precipitation (P) and mean air temperature (TMEAN) trends as a function of elevation expressed in [%/decade], [%/decade] and [°C/decade], respectively. Each point represents one station. Points with lines indicate the trend with the associated 95% confidence interval. Full dots indicate significant trends.

values, while TMEAN anomalies are calculated by subtracting the long-term mean from every time series. Thus, for each year, a centered 21-year moving average is calculated considering the 10 years before and after. We did test other time windows (e.g., 11-year, 31-year), but we find the 21-year window to be the best compromise between a strong noisy signal (11-year) and a too smooth one (31-year). Figure 7 shows the 21-year moving average anomalies of seasonal HN, P and TMEAN for the three regions with respect to the 1920–2020 long-term averages. For HN, until the 1980s, anomalies are positive in all three regions. In all cases, HN anomalies reach a peak of around +25% during the 1970s. Afterward, the anomalies decrease until they become negative. This shift is very evident in the SW and SE regions, where average anomalies change from +25% and +23% to –30% and –23%, respectively. HN decreases at a smaller rate in the N region, where anomalies vary from +24% to –20%. Note that, in the SE region, Udine (113 m a.s.l.) has a more extreme behaviour compared to the other stations. It shows strongly positive anomalies up to the 1960s, with a peak of +86% in the season 1947–1948, and then, starting from the season 1979–1980, negative anomalies are registered.

Considering P, the SW and SE regions show a reduction of up to 10% between the 1980s and 2000s. Another period with negative P anomalies is between the 1940s and 1960s for the SW region and at the end of the 1940s for the SE region. However, for the N region, P has slightly increased over the decades, registering positive anomalies over the last 20 years, with a slight reduction toward values closer to the long-term average in the 2000s. In all cases, a period with more P is between

the 1960s and 1980s. The time series of TMEAN trends are similar in the three regions, with a moderate increase since 1970s and a stronger increase in the last 40 years, when TMEAN anomalies have moved from slightly negative values to  $\sim +1^{\circ}\text{C}$ .

#### 4.4 | Correlation

To better understand which factor plays a major role in controlling HN trends, we calculate the rank correlations between HN and P, TMEAN, NAO, AO, and AMO grouped by the three regions (Figure 8). As expected, the correlation between HN and P increases with elevation, while the correlation between HN and TMEAN tends to zero at the highest stations, suggesting that TMEAN is a limiting factor at low levels, while HN at high elevations is mainly controlled by P. The mean correlation values between HN and P (TMEAN) are: +0.27 (–0.38), +0.36 (–0.57), and +0.46 (–0.41) for the SW, SE, and N regions, respectively. The correlation between HN and NAO, and AO shows the strongest negative correlations for the low-elevation stations in the SW and SE regions, with mean values of –0.37 and –0.41 for NAO, and –0.53 and –0.50 for AO, respectively. This result suggests that for low-elevation regions the presence of specific circulations associated with negative NAO and AO phase is crucial for the occurrence of abundant HN. On the other hand, little or no correlation is found between HN and the AMO index for all regions.

The temporal evolution of the correlations is analysed from the 21-year moving average of the rank correlations between HN and P, TMEAN, NAO, AO, and AMO. For

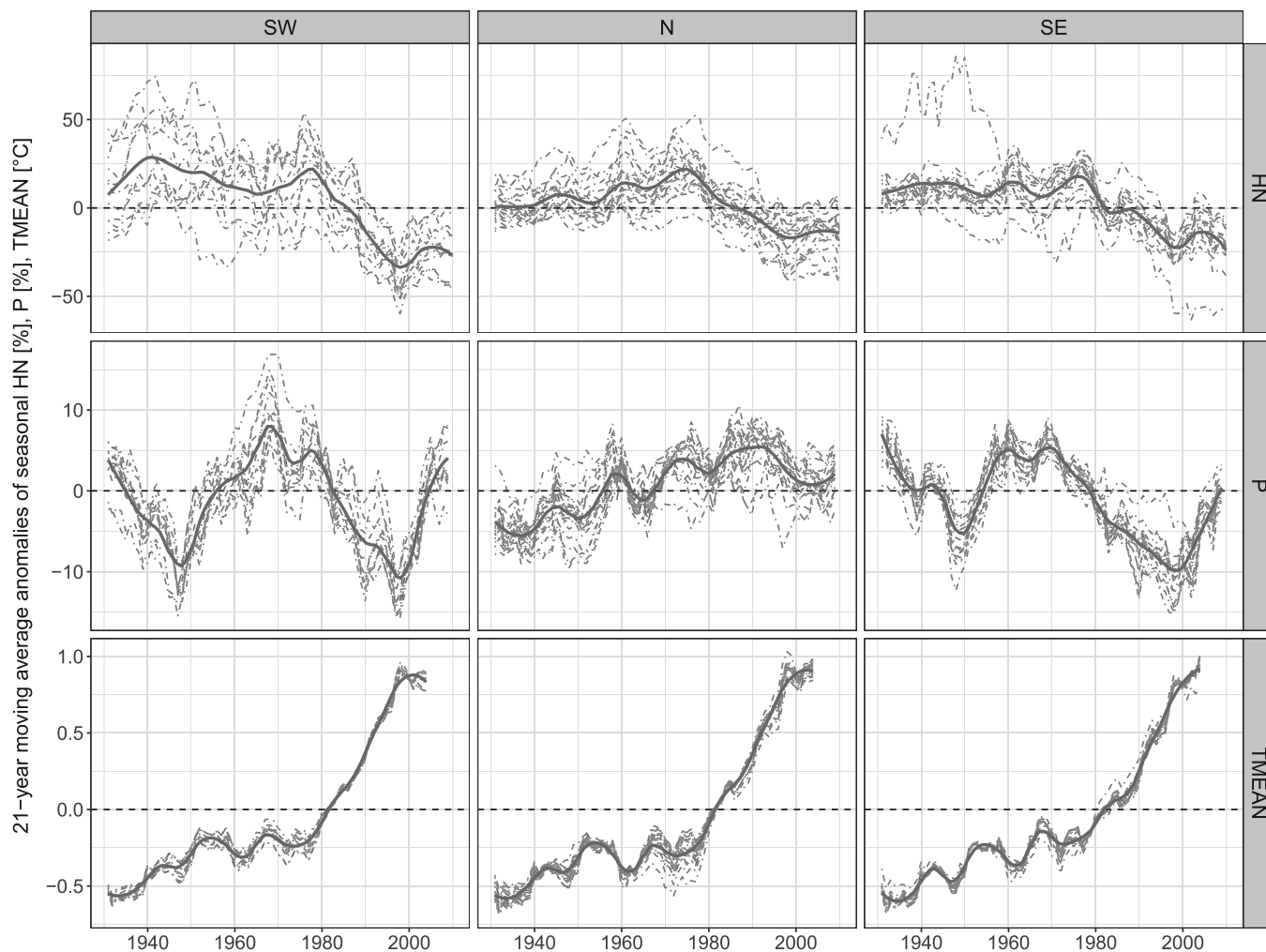


FIGURE 7 21-year moving average anomalies of seasonal snowfall (HN), precipitation (P) and mean air temperature (TMEAN) (blue) for the 1920–2020 period. The red bold thick line indicates the local polynomial regression fitting.

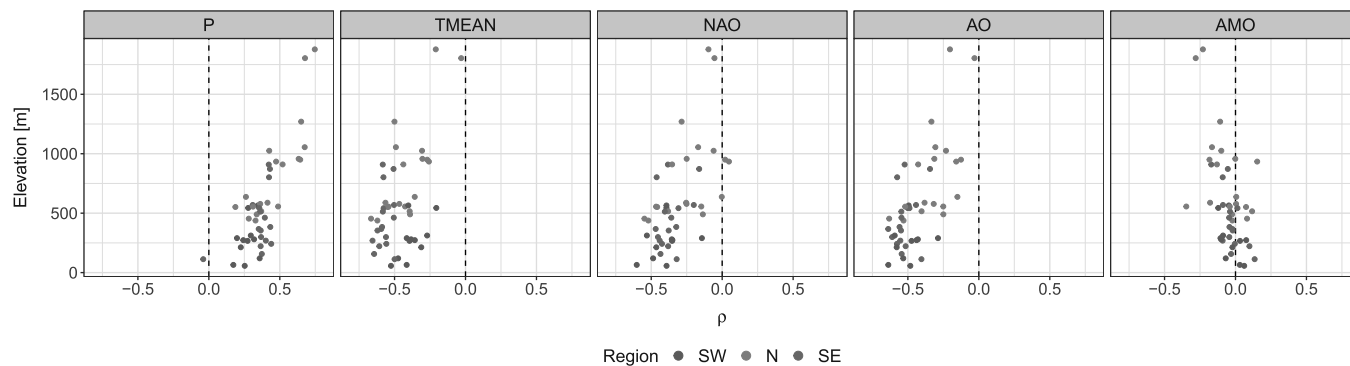
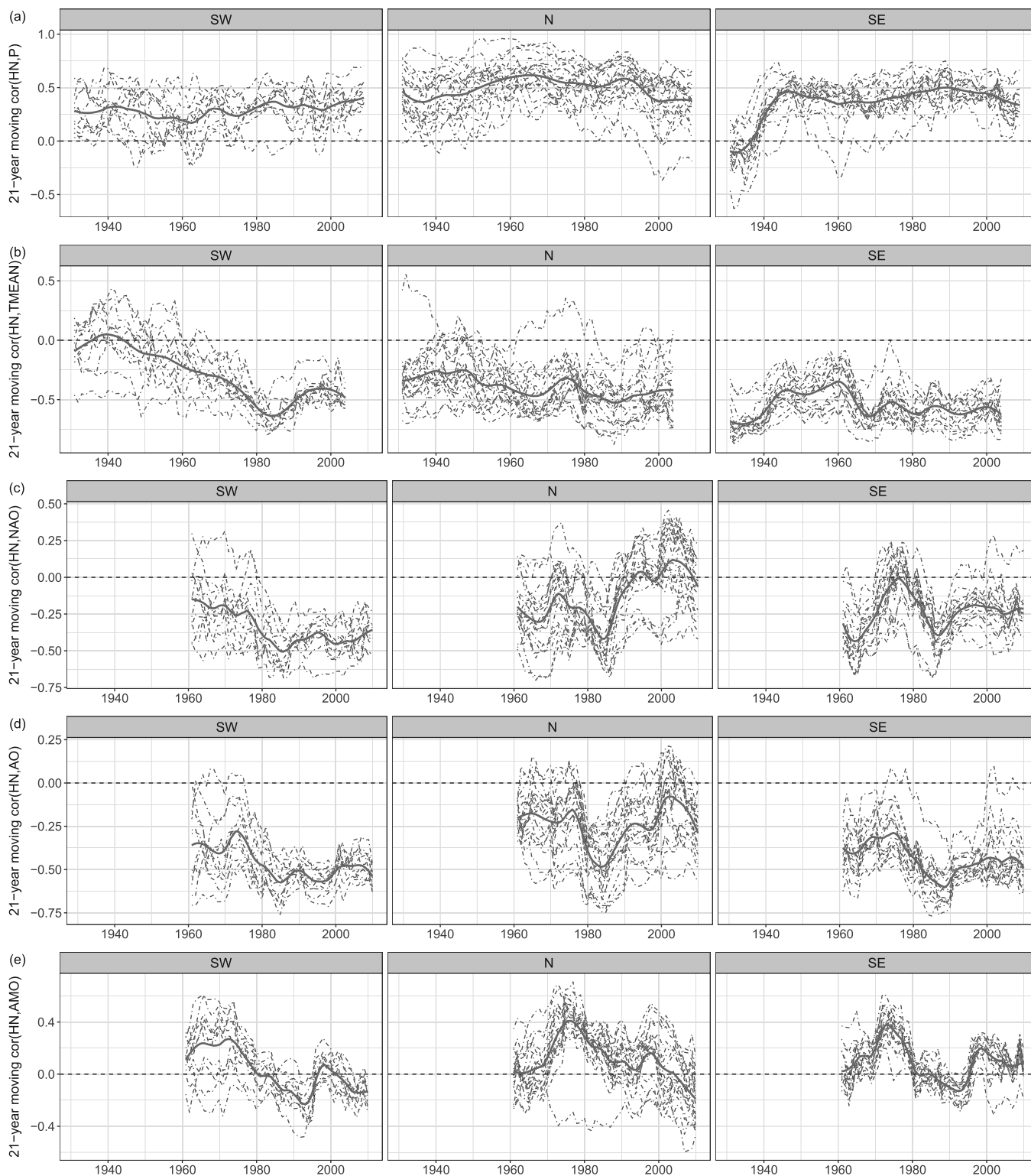


FIGURE 8 Rank correlation between snowfall (HN) and precipitation (P), mean air temperature (TMEAN), North Atlantic Oscillation index (NAO), Arctic Oscillation index (AO) and Atlantic Multidecadal Oscillation index (AMO) grouped by region.

the SW region, the correlation between HN and TMEAN has become more negative over the years. Around the 1940s, for almost all stations, the correlation was 0, while

afterwards the value gradually decreased until it reached a minimum of  $-0.62$  in the 1980s and remained more or less in the same range for the following years (Figure 9).



**FIGURE 9** 21-year moving average of the rank correlation between snowfall (HN) and precipitation (P), mean air temperature (TMEAN), North Atlantic Oscillation index (NAO), Arctic Oscillation index (AO) and Atlantic Multidecadal Oscillation index (AMO) (black). The red bold thick line indicates the local polynomial regression fitting.

The correlation of HN with the NAO and AO indices has also become more marked, settling on average at  $-0.5$ . A similar behaviour can also be observed for the SE region, except that TMEAN correlations were already moderate

from the early period. Instead, in the N region the correlation with the circulation indices is lower, due to a different type of circulation that brings snow over this region (see Section 3, Regionalization). On the other

hand, the correlation between HN and P is more stable and has remained between 0.3 and 0.5 for all regions, except for a short period with lower values in the SE region in the 1930s. Finally, regarding the correlation with the AMO index, it can be seen that in recent years this has been near zero, but with a period of higher correlation in the 1970s, when the N region recorded a peak of 0.4.

## 5 | DISCUSSION

This study has shown that in the last 100 years, seasonal HN has experienced a considerable reduction in most of the analysed locations covering the whole Alpine region. This result has been highlighted in many recent studies at the regional level, but in this study observed HN records have been analysed for a long period (100 years) and for the entire Alpine region. However, a limitation of this study is that most of the analysed stations are located below 1000 m a.s.l., as at higher elevations it is much more difficult to have long and continuous HN observations. To overcome this problem, other studies have analysed HS or SWE. For example, Colombo et al. (2022) modelled SWE using daily HS data obtained from 19 historical stations located in the southern European Alps (Italy) covering an elevation range from 750 to 2600 m a.s.l. They analysed extended-term (1930–2020) fluctuations in the monthly Standardized SWE Index (SSWEI) and investigated its associations with climate change and large-scale atmospheric forcings through teleconnection indices. Their results confirm highly negative trend values of SSWEI in the last few decades (1991–2020) and indicated the increase in TMEAN as the main driver.

Other studies have investigated HN trends, albeit for shorter periods, considering the complex interactions between climate change and the unique geography of the Alpine region. Considering more than 100 observed HN time series located over the northeastern part of Italy, Bertoldi et al. (2023) have shown how seasonal HN trends are negative in the period 1980–2020, especially at the lowest elevations, while some positive trends have been found above 2000 m a.s.l. This result confirmed the findings referring to extreme HN events simulated for the French Alps presented by Roux et al. (2021), who showed that the majority of trends are negative below 2000 m a.s.l. and positive above that altitude. In our analysis we also found a slightly positive trend for the high altitude station of Arosa (1878 m a.s.l.) in the N region. A possible explanation for this result could be linked to the combination of a slight increase in P in the N region together with generally low winter temperatures at high altitudes, despite the significant warming trend.

In this regard, our analysis highlighted that the most negative trends are found for the stations located at the lowest elevations, where TMEAN is increasingly becoming a limiting factor for HN, due to its strong increasing trend (Figure 8). This is particularly true for the low-elevation stations in the SW region, which, as can be seen from the climatology (Figure 4), presents a higher TMEAN than the stations at the same elevation in the SE region (Chimani et al., 2013). Furthermore, it has to be noted that the weather patterns at the origin of HN in the two regions are significantly different. In the SW region, these almost exclusively occur with frontal systems associated with Mediterranean southerly winds, leading to milder conditions which (in a context of long-term atmospheric warming) more and more often cause rain rather than snow to fall at lower altitudes. Instead, in the SE region, HN—although decreasing everywhere—remains relatively easier to observe because it is often associated with longer persistence of cold inversional air layers and cold air flows coming from the northeast or east, weather patterns that are marginal for the development of snow events south of the Alps.

Thanks to the availability of centennial series, it was possible to analyse how, until the 1980s, positive HN anomalies were recorded in all the three regions, with a peak in the 1970s. Afterwards, the anomalies started to change sign, passing from positive to negative, indicating the presence of less snow during winter, especially in the SW and SE regions. The reason for this is to be found in the TMEAN anomalies, as suggested also by Farinotti et al. (2015), Laternser and Schneebeli (2003), Marty (2008), and Mote et al. (2018). As highlighted in the results section, starting from the 1980s, TMEAN anomalies in all the three regions began to rise considerably, reaching values of almost  $+1^{\circ}\text{C}$  compared to the centennial average of the stations themselves. Another factor that can explain the reduction in HN since the 1980s is the reduction in winter P in recent decades, especially for SW and SE regions. This corresponds to a probable global atmospheric circulation regime shift (Reid et al., 2016). Moreover, while P returns to the long-term average after 2000 in the SW and SE regions, HN does not increase and remains below the long-term average, highlighting the crucial contribution of climate warming. In fact, after the 1980s, the limiting factor for HN is mainly TMEAN, especially at low elevations, as shown in Bertoldi et al. (2023).

The correlation analysis shows that the contribution of NAO and AO is different from the contribution of AMO. For the lowest stations of the SW and SE regions, NAO and AO have a moderate correlation ( $-0.5$ ) with HN, while AMO does not show any correlation. The connection between HN and NAO, and AO has been proved

also by Beniston (1997) and Kim et al. (2013). They highlighted that periods with relatively low snow amounts and duration are closely linked to the anomalies of the NAO index. An interesting result we found is that, starting from the 1980s, especially for the SW region, the NAO and AO indices began to have a higher correlation with HN. A possible explanation is that, due to the rise in TMEANs starting from the 1980s, the favourable combination of more drivers (TMEAN, P and atmospheric circulation) is needed for HN occurrence. This regional strong correlation between HN events and the NAO and AO indices might be exploited to improve long-term HN forecasts in the Alps. Finally, the absence of correlation between HN and AMO can be explained considering that this index influences P and TMEAN mainly in spring and less during wintertime (Zampieri et al., 2017).

## 6 | CONCLUSIONS

This study analysed 46 long-term series of snowfall (HN) observations during the period 1920–2020 over the whole Alpine domain. After a check on quality, homogeneity and gaps, HN trends were identified using the Sen's slope estimator and the Mann–Kendall trend test, and compared with trends of precipitation (P) and mean air temperature (TMEAN). Moreover, also large-scale predictors, that is, the North Atlantic Oscillation (NAO), Arctic Oscillation (AO) and Atlantic Multidecadal Oscillation (AMO) indices were considered. Data have been grouped in three sub-regions: South-West (SW), South-East (SE) and North (N).

Negative seasonal HN trends are found in all the three regions, especially for the SW and SE regions, with overall values of  $-4.9$  and  $-3.8\%/decade$ , respectively. Only three positive trends are found and all are in the N region, which recorded on average a trend of  $-2.3\%/decade$ . Since the average elevation of the stations analysed in this region is the highest of the three, this suggests that the decrease in HN is particularly affecting the lower elevations, while the higher ones suffer less. This is also confirmed by the analysis of trends as a function of elevation, which shows that stations at lower altitudes have larger negative trends than those at higher elevations. The main factor responsible for the reduction in HN is TMEAN, which for all stations shows a positive or strongly positive and statistically significant trend with an overall value of  $+0.16^\circ\text{C}/decade$ . A slight increase in winter precipitation is detected, especially for the N region, which can partially explain the few positive HN trends found in this area. In fact, despite the temperature increase, at certain elevations the average winter temperatures are still sufficiently low to allow HN to occur. For

both P and TMEAN, no elevation dependency has been found.

By looking at how trends have changed over the past 100 years, this study has revealed that the sharp decline in HN has mainly occurred over the last 40 years. Until the 1980s, HN anomalies remained at consistently positive values, and only afterwards they started to decrease. This occurred for all the three regions. Clearly, the key role in this steep decline was played by TMEAN, which has increased significantly since the 1980s. On the other hand, the role of P is more difficult to interpret. For the SW and SE region, for example, a cyclical pattern can be seen and it seems to have influenced HN only from the 1980s, when both negative HN and P anomalies were recorded. Instead, for the N region, it can be seen that HN and P anomalies have a similar behaviour until the 1980s, but then start to diverge, suggesting that also in this region TMEAN starts to become the main limiting factor for HN.

This study also showed that there is a positive correlation ( $>0.5$ ) between HN and P for stations in the N region above 1000 m a.s.l., suggesting that in winter P is in the form of snow in most cases. As elevation decreases, the correlation decreases too. Instead, an opposite behaviour has been found for the correlation between HN and TMEAN, NAO, AO: stations at lower elevations are better correlated than stations at higher elevations. This suggests that, at low elevation, the combination of TMEAN and atmospheric circulation is more crucial for HN occurrence than at higher elevation. However, this correlation has increased since the 1980s, suggesting that TMEAN has become an increasingly limiting factor for HN in the last 40 years, especially in the SW and SE regions. No correlation between HN and AMO has been found, neither looking at the entire period nor over time.

Our study is among a few that consider 100 years of HN data from over 40 stations over all the Alps. The method used to check the spatial consistency and homogeneity of HN data proved to be extremely useful in assessing the quality of the series and, in the future, it could enable more robust studies of HN in other areas. In the future, the quality-check analysis can be extended to higher temporal resolutions, such as monthly or daily values. The assessment of HN series and their trends adds valuable information to that derived from other snow-related parameters, such as snow depth (HS), snow cover area (SCA) or snow water equivalent (SWE). The integrated analysis based on multiple snow-related variables and high-quality and dense observation databases can provide a more comprehensive picture of snow cover changes and can be used for a wide range of applications, such as the validation of climatic reanalyses, snow hydrological models or remote sensing products.

## AUTHOR CONTRIBUTIONS

**Michele Bozzoli:** Writing – review and editing; writing – original draft; visualization; data curation; software; methodology; conceptualization; investigation; validation; formal analysis. **Alice Crespi:** Methodology; validation; supervision; writing – review and editing; data curation; conceptualization; formal analysis. **Michael Matiu:** Methodology; data curation; validation; formal analysis; supervision; writing – review and editing; conceptualization. **Bruno Majone:** Writing – review and editing; project administration; resources; supervision; conceptualization; funding acquisition. **Lorenzo Giovannini:** Writing – review and editing; supervision; conceptualization; methodology; validation; formal analysis; data curation. **Dino Zardi:** Conceptualization; supervision; resources; project administration; writing – review and editing; funding acquisition. **Yuri Brugnara:** Conceptualization; supervision; writing – review and editing; methodology; visualization; validation; investigation. **Alessio Bozzo:** Conceptualization; writing – review and editing; supervision; visualization; methodology; validation; investigation. **Daniele Cat Berro:** Writing – review and editing; supervision. **Luca Mercalli:** Writing – review and editing; supervision. **Giacomo Bertoldi:** Conceptualization; funding acquisition; visualization; writing – review and editing; project administration; resources; supervision; methodology.

## ACKNOWLEDGEMENTS

We acknowledge for their support on data providing Walter Beozzo, Alberto Trenti, Mauro Gaddo (Meteo-trentino and civil protection department of the Autonomous Province of Trento); Matteo Calzà, Filippo Orlando, (Association MeteoTrentinoAltoAdige); Pamela Turchiarulo (Meteorological Observatory Foundation of Milano—Duomo); Marco Pifferetti, Roberto Ghiselli, Pierluigi Randi (“LA NEVE IN PIANURA PADANA NELLA CLIMATOLOGIA E NELLA STORIA”—Ronca Editore); Alpine—Adriatic Meteorological Society; Meteorological Observatory of Parma; Gregor Vertačnik (Meteorology Office—Slovenian Environment Agency). Open access publishing facilitated by Università degli Studi di Trento, as part of the Wiley - CRUI-CARE agreement.

## FUNDING INFORMATION

Università degli Studi di Trento, Eurac Research, Swiss National Science Foundation (SNSF) and Autonomous Province of Bolzano (Italy), SnowTinel project: “Sentinel-1 SAR assisted catchment hydrology: toward an improved snow-melt dynamics for alpine regions.” Contract No. D55F21005230003.










## CONFLICT OF INTEREST STATEMENT

The authors declare no conflict of interest.

## DATA AVAILABILITY STATEMENT

Data will be made available on request, and, for those with no restrictions, published in an open dataset.

## ORCID

**Michele Bozzoli**  <https://orcid.org/0000-0002-3844-0701>  
**Alice Crespi**  <https://orcid.org/0000-0003-4186-8474>  
**Michael Matiu**  <https://orcid.org/0000-0001-5289-0592>  
**Bruno Majone**  <https://orcid.org/0000-0003-3471-7408>  
**Lorenzo Giovannini**  <https://orcid.org/0000-0003-1650-0344>  
**Dino Zardi**  <https://orcid.org/0000-0002-3573-3920>  
**Yuri Brugnara**  <https://orcid.org/0000-0001-8427-0064>  
**Alessio Bozzo**  <https://orcid.org/0000-0002-8069-3809>  
**Giacomo Bertoldi**  <https://orcid.org/0000-0003-0397-8103>

## REFERENCES

- Aby, A.Z., Melesse, A.M., Seyoum, W.M. & Abtew, W. (2019) Drought and climate teleconnection and drought monitoring. In: *Extreme hydrology and climate variability*. Amsterdam, Netherlands: Elsevier, pp. 275–295. Available from: <https://doi.org/10.1016/B978-0-12-815998-9.00022-1>
- Alexandersson, H. & Moberg, A. (1997) Homogenization of Swedish temperature data. Part I: homogeneity test for linear trends. *International Journal of Climatology*, 17(1), 25–34.
- Aragon, C.M. & Hill, D.F. (2024) Changing snow water storage in natural snow reservoirs. *Hydrology and Earth System Sciences*, 28(4), 781–800. Available from: <https://doi.org/10.5194/hess-28-781-2024>
- Auer, I., Böhm, R., Jurkovic, A., Lipa, W., Orlik, A., Potzmann, R. et al. (2007) Histalp—historical instrumental climatological surface time series of the greater alpine region. *International Journal of Climatology*, 27(1), 17–46. Available from: <https://doi.org/10.1002/joc.1377>
- Auer, I., Böhm, R., Jurković, A., Orlik, A., Potzmann, R., Schöner, W. et al. (2005) A new instrumental precipitation dataset for the greater alpine region for the period 1800–2002. *International Journal of Climatology*, 25(2), 139–166. Available from: <https://doi.org/10.1002/joc.1135>
- Barnett, T.P., Pierce, D.W., Hidalgo, H.G., Bonfils, C., Santer, B.D., Das, T. et al. (2008) Human-induced changes in the hydrology of the western United States. *Science*, 319(5866), 1080–1083.
- Baronetti, A., Fratianni, S., Acquavotta, F. & Fortin, G. (2019) A quality control approach to better characterize the spatial distribution of snow depth over New Brunswick, Canada. *International Journal of Climatology*, 39(14), 5470–5485. Available from: <https://doi.org/10.1002/joc.6166>
- Bartolini, E., Claps, P. & D’Odorico, P. (2010) Connecting European snow cover variability with large scale atmospheric patterns. *Advances in Geosciences*, 26, 93–97.
- Bavay, M., Lehning, M., Jonas, T. & Löwe, H. (2009) Simulations of future snow cover and discharge in alpine headwater

- catchments. *Hydrological Processes: An International Journal*, 23(1), 95–108. Available from: <https://doi.org/10.1002/hyp.7195>
- Beniston, M. (1997) Variations of snow depth and duration in the swiss Alps over the last 50 years: links to changes in large-scale climatic forcings. In: *Climatic change at high elevation sites*. Berlin, Germany: Springer, pp. 49–68.
- Beniston, M. (2012) Impacts of climatic change on water and associated economic activities in the swiss Alps. *Journal of Hydrology*, 412, 291–296. Available from: <https://doi.org/10.1016/j.jhydrol.2010.06.046>
- Beniston, M., Farinotti, D., Stoffel, M., Andreassen, L.M., Coppola, E., Eckert, N. et al. (2018) The European mountain cryosphere: a review of its current state, trends, and future challenges. *The Cryosphere*, 12(2), 759–794. Available from: <https://doi.org/10.5194/tc-12-759-2018>
- Bertoldi, G., Bozzoli, M., Crespi, A., Matiu, M., Giovannini, L., Zardi, D. et al. (2023) Diverging snowfall trends across months and elevation in the northeastern Italian Alps. *International Journal of Climatology*, 43(6), 2794–2819. Available from: <https://doi.org/10.1002/joc.8002>
- Brown, R.D. & Mote, P.W. (2009) The response of northern hemisphere snow cover to a changing climate. *Journal of Climate*, 22(8), 2124–2145. Available from: <https://doi.org/10.1175/2008JCLI2665.1>
- Buchmann, M., Coll, J., Aschauer, J., Begert, M., Brönnimann, S., Chimani, B. et al. (2022) Homogeneity assessment of swiss snow depth series: comparison of break detection capabilities of (semi-) automatic homogenization methods. *The Cryosphere*, 16(6), 2147–2161. Available from: <https://doi.org/10.5194/tc-16-2147-2022>
- Carrer, M., Dibona, R., Prendin, A.L. & Brunetti, M. (2023) Recent waning snowpack in the Alps is unprecedented in the last six centuries. *Nature Climate Change*, 13(2), 155–160. Available from: <https://doi.org/10.1038/s41558-022-01575-3>
- Causinus, H. & Mestre, O. (2004) Detection and correction of artificial shifts in climate series. *Journal of the Royal Statistical Society Series C: Applied Statistics*, 53(3), 405–425.
- Chimani, B., Matulla, C., Böhm, R. & Hofstätter, M. (2013) A new high resolution absolute temperature grid for the greater alpine region back to 1780. *International Journal of Climatology*, 33(9), 2129–2141. Available from: <https://doi.org/10.1002/joc.3574>
- Coll, J., Domonkos, P., Guijarro, J., Curley, M., Rustemeier, E., Aguilar, E. et al. (2020) Application of homogenization methods for Ireland's monthly precipitation records: comparison of break detection results. *International Journal of Climatology*, 40(14), 6169–6188. Available from: <https://doi.org/10.1002/joc.6575>
- Colombo, N., Valt, M., Romano, E., Salerno, F., Godone, D., Cianfarra, P. et al. (2022) Long-term trend of snow water equivalent in the Italian Alps. *Journal of Hydrology*, 614, 128532. Available from: <https://doi.org/10.1016/j.jhydrol.2022.128532>
- Diodato, N., Bertolin, C., Bellocchi, G., De Ferri, L. et al. (2020) New insights into the world's longest series of monthly snowfall (Parma, northern Italy, 1777–2018). *International Journal of Climatology*, 41(Supp.1), E1270–E1286. Available from: <https://doi.org/10.1002/joc.6766>
- Domonkos, P. (2011) Adapted Causinus-Mestre algorithm for networks of temperature series (ACMANT). *International Journal of Geosciences*, 2(3), 293–309. Available from: <https://doi.org/10.4236/ijg.2011.23032>
- Durand, Y., Giraud, G., Laternser, M., Etchevers, P., Mérindol, L. & Lesaffre, B. (2009) Reanalysis of 47 years of climate in the French Alps (1958–2005): climatology and trends for snow cover. *Journal of Applied Meteorology and Climatology*, 48(12), 2487–2512. Available from: <https://doi.org/10.1175/2009JAMC1810.1>
- Farinotti, D., Longuevergne, L., Moholdt, G., Duethmann, D., Mölg, T., Bolch, T. et al. (2015) Substantial glacier mass loss in the Tien Shan over the past 50 years. *Nature Geoscience*, 8(9), 716–722. Available from: <https://doi.org/10.1038/NNGEO2513>
- Guijarro, J. A. (2018). Homogenization of climatic series with Climatol. *Reporte técnico State Meteorological Agency (AEMET), Balearic Islands Office, Spain*.
- Guo, L. & Li, L. (2015) Variation of the proportion of precipitation occurring as snow in the Tian Shan Mountains, China. *International Journal of Climatology*, 35(7), 1379–1393. Available from: <https://doi.org/10.1002/joc.4063>
- Haberhorn, A. (2019) European snow booklet – an inventory of snow measurements in Europe. *EnviDat*, 10, 1417–1420. Available from: <https://doi.org/10.16904/envidat.59>
- Hunter, T., Tootle, G. & Piechota, T. (2006) Oceanic-atmospheric variability and western US snowfall. *Geophysical Research Letters*, 33(13), L13706, (1–5). Available from: <https://doi.org/10.1029/2006GL026600>
- Hurrell, J.W., Kushnir, Y., Ottersen, G. & Visbeck, M. (2003) An overview of the North Atlantic oscillation. *Geophysical Monograph-American Geophysical Union*, 134, 1–36. Available from: <https://doi.org/10.1029/134GM01>
- Isotta, F., Chimani, B., Hiebl, J. & Frei, C. (2024) Long-term alpine precipitation reconstruction (LAPrec): a gridded monthly data set dating back to 1871. *Journal of Geophysical Research: Atmospheres*, 129(2), 1–18. Available from: <https://doi.org/10.1029/2023JD039637>
- Isotta, F., Frei, C., Weilguni, V., Perčec Tadić, M., Lassegues, P., Rudolf, B. et al. (2014) The climate of daily precipitation in the Alps: development and analysis of a high-resolution grid dataset from pan-alpine rain-gauge data. *International Journal of Climatology*, 34(5), 1657–1675. Available from: <https://doi.org/10.1002/joc.3794>
- Kendall, M. (1975) *Rank correlation methods*. London, UK: Griffin.
- Kim, Y., Kim, K.-Y. & Kim, B.-M. (2013) Physical mechanisms of European winter snow cover variability and its relationship to the NAO. *Climate Dynamics*, 40(7), 1657–1669. Available from: <https://doi.org/10.1007/s00382-012-1365-5>
- Laternser, M. & Schneebeli, M. (2003) Long-term snow climate trends of the swiss Alps (1931–99). *International Journal of Climatology*, 23(7), 733–750. Available from: <https://doi.org/10.1002/joc.912>
- Leporati, E. & Mercalli, L. (1994) Snowfall series of Turin, 1784–1992: climatological analysis and action on structures. *Annals of Glaciology*, 19, 77–84.
- Luna, M., Guijarro, J. & López, J. (2012) A monthly precipitation database for Spain (1851–2008): reconstruction, homogeneity and trends. *Advances in Science and Research*, 8(1), 1–4. Available from: <https://doi.org/10.5194/asr-8-1-2012>
- Mann, H. (1945) Nonparametric tests against trend. *Journal of the Econometric Society*, 13, 245–259.
- Marcolini, G., Bellin, A. & Chiogna, G. (2017) Performance of the standard Normal homogeneity test for the homogenization of mean seasonal snow depth time series. *International Journal of Climatology*, 37, 1267–1277. Available from: <https://doi.org/10.1002/joc.4977>



- Marcolini, G., Koch, R., Chimani, B., Schöner, W., Bellin, A., Disse, M. et al. (2019) Evaluation of homogenization methods for seasonal snow depth data in the Austrian Alps, 1930–2010. *International Journal of Climatology*, 39(11), 4514–4530. Available from: <https://doi.org/10.1002/joc.6095>
- Marke, T., Hanzer, F., Olefs, M. & Strasser, U. (2018) Simulation of past changes in the Austrian snow cover 1948–2009. *Journal of Hydrometeorology*, 19(10), 1529–1545. Available from: <https://doi.org/10.1175/JHM-D-17-0245.1>
- Marty, C. (2008) Regime shift of snow days in Switzerland. *Geophysical Research Letters*, 35(12), L12501, (1–5). Available from: <https://doi.org/10.1029/2008GL033998>
- Marty, C., Rohrer, M.B., Huss, M. & Stähli, M. (2023) Multi-decadal observations in the Alps reveal less and wetter snow, with increasing variability. *Frontiers in Earth Science*, 11, 1165861. Available from: <https://doi.org/10.3389/feart.2023.1165861>
- Marty, C., Tilg, A.-M. & Jonas, T. (2017) Recent evidence of large-scale receding snow water equivalents in the European Alps. *Journal of Hydrometeorology*, 18(4), 1021–1031. Available from: <https://doi.org/10.1175/JHM-D-16-0188.1>
- Matiu, M., Crespi, A., Bertoldi, G., Carmagnola, C.M., Marty, C., Morin, S. et al. (2021) Observed snow depth trends in the European Alps: 1971 to 2019. *The Cryosphere*, 15(3), 1343–1382. Available from: <https://doi.org/10.5194/tc-15-1343-2021>
- Milner, A.M., Khamis, K., Battin, T.J., Brittain, J.E., Barrand, N.E., Füreder, L. et al. (2017) Glacier shrinkage driving global changes in downstream systems. *Proceedings of the National Academy of Sciences*, 114(37), 9770–9778. Available from: <https://doi.org/10.1073/pnas.1619807114>
- Monteiro, D. & Morin, S. (2023) Multi-decadal analysis of past winter temperature, precipitation and snow cover data in the European Alps from reanalyses, climate models and observational datasets. *The Cryosphere*, 17(8), 3617–3660. Available from: <https://doi.org/10.5194/tc-17-3617-2023>
- Morin, S., Samacoïts, R., François, H., Carmagnola, C.M., Abegg, B., Demiroglu, O.C. et al. (2021) Pan-European meteorological and snow indicators of climate change impact on ski tourism. *Climate Services*, 22, 100215. Available from: <https://doi.org/10.1016/j.cliser.2021.100215>
- Mote, P.W., Li, S., Lettenmaier, D.P., Xiao, M. & Engel, R. (2018) Dramatic declines in snowpack in the western US. *Npj Climate and Atmospheric Science*, 1(1), 2. Available from: <https://doi.org/10.1038/s41612-018-0012-1>
- Olefs, M., Koch, R., Hiebl, J., Haslinger, K. & Schöner, W. (2017) Seasonal snow cover evolution in the Nationalparks Austria since 1961. *6th Symposium for Research in Protected Areas*, 1, 475–478.
- Olefs, M., Koch, R., Schöner, W. & Marke, T. (2020) Changes in snow depth, snow cover duration, and potential snowmaking conditions in Austria, 1961–2020—a model based approach. *Atmosphere*, 11(1), 7600. Available from: <https://doi.org/10.3390/atmos11121330>
- Perovich, D.K. (2007) Light reflection and transmission by a temperate snow cover. *Journal of Glaciology*, 53(181), 201–210. Available from: <https://doi.org/10.3189/172756507782202919>
- Qi, W., Feng, L., Liu, J. & Yang, H. (2020) Snow as an important natural reservoir for runoff and soil moisture in Northeast China. *Journal of Geophysical Research: Atmospheres*, 125(22), 1–15. Available from: <https://doi.org/10.1029/2020JD033086>
- R Core Team. (2020) *R: a language and environment for statistical computing*. Vienna, Austria: R Foundation for Statistical Computing. Available from: <http://www.R-project.org>
- Reid, P.C., Hari, R.E., Beaugrand, G., Livingstone, D.M., Marty, C., Straile, D. et al. (2016) Global impacts of the 1980s regime shift. *Global Change Biology*, 22(2), 682–703. Available from: <https://doi.org/10.1111/gcb.13106>
- Resch, G., Koch, R., Marty, C., Chimani, B., Begert, M., Buchmann, M. et al. (2023) A quantile-based approach to improve homogenization of snow depth time series. *International Journal of Climatology*, 43(1), 157–173. Available from: <https://doi.org/10.1002/joc.7742>
- Rixen, C., Teich, M., Lardelli, C., Gallati, D., Pohl, M., Pütz, M. et al. (2011) Winter tourism and climate change in the Alps: an assessment of resource consumption, snow reliability, and future snowmaking potential. *Mountain Research and Development*, 31(3), 229–236. Available from: <https://doi.org/10.1659/MRD-JOURNAL-D-10-00112.1>
- Rolland, C. (2003) Spatial and seasonal variations of air temperature lapse rates in alpine regions. *Journal of Climate*, 16(7), 1032–1046.
- Roux, E.L., Evin, G., Eckert, N., Blanchet, J. & Morin, S. (2021) Elevation-dependent trends in extreme snowfall in the French Alps from 1959 to 2019. *The Cryosphere*, 15(9), 4335–4356. Available from: <https://doi.org/10.5194/tc-15-4335-2021>
- Sen, P.K. (1968) Estimates of the regression coefficient based on Kendall's tau. *Journal of the American Statistical Association*, 63(324), 1379–1389.
- Serquet, G., Marty, C., Dulej, J.-P. & Rebetez, M. (2011) Seasonal trends and temperature dependence of the snowfall/precipitation day ratio in Switzerland. *Geophysical Research Letters*, 38(7), L07703, (1–5). Available from: <https://doi.org/10.1029/2011gl046976>
- Tomasi, E., Giovannini, L., Zardi, D. & de Franceschi, M. (2017) Optimization of Noah and Noah\_M PWF land surface schemes in snow-melting conditions over complex terrain. *Monthly Weather Review*, 145(12), 4727–4745. Available from: <https://doi.org/10.1175/MWR-D-16-0408.1>
- Valt, M. & Cianfarra, P. (2010) Recent snow cover variability in the Italian Alps. *Cold Regions Science and Technology*, 64(2), 146–157. Available from: <https://doi.org/10.1016/j.coldregions.2010.08.008>
- Zampieri, M., Toreti, A., Schindler, A., Scoccimarro, E. & Gualdi, S. (2017) Atlantic multi-decadal oscillation influence on weather regimes over Europe and the Mediterranean in spring and summer. *Global and Planetary Change*, 151, 92–100. Available from: <https://doi.org/10.1016/j.gloplacha.2016.08.014>
- Zhuravleva, T.B. & Kokhanovsky, A.A. (2011) Influence of surface roughness on the reflective properties of snow. *Journal of Quantitative Spectroscopy and Radiative Transfer*, 112(8), 1353–1368. Available from: <https://doi.org/10.1016/j.jqsrt.2011.01.004>

**How to cite this article:** Bozzoli, M., Crespi, A., Matiu, M., Majone, B., Giovannini, L., Zardi, D., Brugnara, Y., Bozzo, A., Berro, D. C., Mercalli, L., & Bertoldi, G. (2024). Long-term snowfall trends and variability in the Alps. *International Journal of Climatology*, 44(13), 4571–4591. <https://doi.org/10.1002/joc.8597>

## APPENDIX A: SNOWFALL STATIONS META DATA

**TABLE A1** List of the snowfall (HN) stations used. For each stations are indicated ID number (ID), provider (Prov), station name (Name), longitude (Long), latitude (Lat), elevation (Elev), start year (SY), end year (EY), use (Use). H indicates HN stations used only for homogenization, while HT for both homogenization and trend analysis.

ID	Prov	Name	Long (°)	Lat (°)	Elev (m)	SY	EY	Use
1	IT SMI	Aosta	7.3334	45.728	544	1891	2019	HT
2	CH METEOSWISS	Arosa	9.679	46.7926	1878	1890	2020	HT
3	AT GSA	Bad Bleiberg	13.6844	46.6253	909	1896	2022	HT
4	AT GSA	Bad Gleichenberg	15.9036	46.8722	269	1861	2022	HT
5	CH METEOSWISS	Bern Zollikofen	7.464	46.9907	552	1897	2020	HT
6	IT SMI	Bra	7.8519	44.701	290	1862	2018	HT
7	AT GSA	Bregenz	9.7461	47.4992	424	1869	2022	H
8	AT GSA	Bruck Mur	15.2497	47.4056	482	1895	2022	H
9	SI ARSO	Celje	15.2259	46.2366	242	1893	2022	HT
10	SI ARSO	Cerknica	14.3634	45.7956	569	1894	2022	HT
11	CH METEOSWISS	Chur	9.5305	46.8704	556	1888	2020	HT
12	CH METEOSWISS	Col du Grand St Bernard	7.1707	45.8691	2472	1865	2020	H
13	SI ARSO	Črnomelj	15.1462	45.56	157	1882	2022	HT
14	IT SMI	Cuneo	7.5478	44.3897	565	1877	2019	HT
15	AT GSA	Deutschlandsberg	15.2269	46.8217	354	1895	2022	HT
16	AT GSA	Doellach	12.9025	46.9581	1071	1871	2022	H
17	IT SMI	Domodossola	8.2877	46.1133	280	1872	2019	HT
18	SI ARSO	Dravograd	15.0283	46.5919	384	1885	2022	HT
19	CH METEOSWISS	Einsiedeln	8.7565	47.133	910	1907	2020	HT
20	CH METEOSWISS	Elm	9.1753	46.9238	957	1881	2020	HT
21	AT GSA	Feldkirch	9.6097	47.2711	438	1875	2022	HT
22	CH METEOSWISS	Glarus	9.0669	47.0346	516	1891	2020	HT
23	AT GSA	Gmunden	13.8075	47.9147	424	1892	2016	H
24	CH METEOSWISS	Goschenen	8.5954	46.6927	950	1901	2020	HT
25	AT GSA	Graz Univ.	15.4489	47.0778	367	1851	2022	H
26	CH METEOSWISS	Guttannen	8.2917	46.6565	1055	1876	2020	HT
27	AT GSA	Hall Admont	14.4908	47.5944	637	1895	2022	HT
28	AT GSA	Innsbruck Univ.	11.3842	47.26	578	1866	2022	HT
29	AT GSA	Klagenfurt Flughafen	14.3183	46.6483	450	1813	2022	H
30	SI ARSO	Kranjska Gora	13.7891	46.4865	802	1895	2022	HT
31	AT GSA	Krimml	12.1819	47.2292	1009	1891	2022	H
32	AT GSA	Kufstein	12.1628	47.5753	490	1905	2022	HT
33	AT GSA	Langen Am Arlberg	10.1247	47.135	1270	1881	2022	HT
34	SI ARSO	Laško	15.2341	46.1565	222	1895	2022	HT
35	AT GSA	Lienz	12.8064	46.8256	661	1895	2022	H
36	SI ARSO	Ljubljana	14.5124	46.0655	299	1895	2022	HT
37	SI ARSO	Luče	14.7457	46.3543	513	1893	2022	HT
38	CH METEOSWISS	Lugano	8.9603	46.0042	273	1864	2020	HT
39	CH METEOSWISS	Luzern	8.301	47.0364	454	1883	2020	HT
40	AT GSA	Mariazell St Sebastian	15.3022	47.7892	864	1889	2022	H
41	CH METEOSWISS	Meiringen	8.1692	46.7322	588	1901	2020	HT
42	AT GSA	Micheldorf	14.1344	47.8831	459	1901	2022	H
43	IT OMD	Milano	9.19	45.4669	120	1881	2020	HT
44	AT GSA	Mondsee	13.3472	47.8508	481	1892	2022	H
45	IT OMP	Parma	10.328	44.8015	57	1867	2021	HT
46	SI ARSO	Planina pri Rakeku	14.2525	45.8308	462	1894	1988	HT
47	AT GSA	Rauris	12.9925	47.2236	934	1875	2022	HT
48	AT GSA	Reichenau Rax	15.837	47.6997	488	1865	2022	H
49	AT GSA	Reichersberg	13.3761	48.3311	351	1881	2022	H
50	AT GSA	Ried Im Innkreis	13.475	48.2172	427	1872	2022	H
51	IT MTAA	Riva del Garda	10.85	45.883	65	1921	2020	HT
52	IT MTAA	Rovereto	11.044	45.897	213	1882	2021	HT
53	AT GSA	Salzburg Flughafen	13.0083	47.7894	430	1874	2022	H
54	AT GSA	Schmittenhoehe	12.7381	47.3286	1956	1880	2022	H
55	AT GSA	Schroekben	10.0861	47.2617	1244	1895	2022	H
56	AT GSA	Seckau	14.7786	47.2708	872	1895	2022	HT
57	CH METEOSWISS	Segl Maria	9.7623	46.4323	1804	1864	2020	HT
58	SI ARSO	Škofja Loka	14.2924	46.172	367	1895	2022	HT
59	SI ARSO	Sodražica	14.6382	45.7629	542	1892	2022	HT
60	AT GSA	Sonnblick Tawes	12.9575	47.0542	3109	1886	2022	H
61	AT GSA	Stift Zwettl	15.2036	48.6178	502	1883	2022	H
62	AT GSA	Stolzalpe	14.1883	47.1231	1291	1921	2022	H
63	AT GSA	Tamsweg	13.8083	47.1331	1025	1895	2022	HT
64	IT SMI	Torino	7.6272	45.0721	267	1787	2020	HT
65	IT MTN	Trento	11.1331	46.0742	312	1920	2020	HT
66	IT SMAA	Udine	13.233333	46.066667	113	1776	2000	HT
67	AT GSA	Villacher Alpe	13.6733	46.6036	2140	1876	2022	H
68	AT GSA	Waidhofen Ybbs	14.8097	47.9456	384	1896	2022	H
69	AT GSA	Wien Hohe warte	16.3564	48.2486	198	1775	2022	H
70	CH METEOSWISS	Zurich Fluntern	8.5657	47.3779	555	1864	2020	HT

## APPENDIX B: HOMOGENEITY CHECK

In this study, the Climatol procedure, as implemented in the R package “climatol” version 3.1.1 (Guijarro, 2018), was used to check the homogeneity of the HN time series. Other procedures could be applied, such as the HOMogenization softwarE in R (HOMER; Caussinus & Mestre, 2004) or the Adapted Caussinus-Mestre Algorithm for Networks of Temperature series (ACMANT; Domonkos (2011)). However, as suggested by Buchmann et al. (2022), HOMER is very time-consuming for the user and also requires extensive expert knowledge. On the other hand, ACMANT is easier to apply, but implies a lot of postprocessing, due to the large number of break points detected, and also requires in-depth knowledge about the station network. Moreover, Coll et al. (2020) recommended Climatol as the method to be used for precipitation, because the identified break points appeared likely to be more realistic than the ones found with either ACMANT or HOMER. Therefore, for these reasons, Climatol was chosen in this study.

Climatol uses composite reference series and detects breaks one-by-one with the Standard Normal Homogenization Test (SNHT; Alexandersson and Moberg (1997)) applied to anomaly series between observed and reference data. Data are normalized based on ratio or difference, depending on the climate variable, with respect to the mean climatological value of the series. The normalization based on the ratio is applied to HN series, since it is more suitable for skewed data. Reference series are

estimated from the nearest observed series based on geographical proximity using Euclidean distances (Luna et al., 2012). Series of anomalies are obtained by subtracting the estimated values from the observed ones (always in normalized form).

When the SNHT statistics of the series are greater than a prescribed threshold, the series is split at the point of maximum SNHT, moving all data before the break to a new series. This procedure is done iteratively, splitting only the series with the higher SNHT values at every cycle, until no series is found inhomogeneous. Since SNHT was originally designed for identifying a single break-point, the existence of two or more shifts in the mean with similar values could mask its results. To minimize this problem, SNHT is applied in a first stage to stepped overlapping temporal windows (stage 1), followed by a second stage applying SNHT to the entire series (stage 2), which is where the test exhibits more power of detection. Finally, a third stage is dedicated to in-fill all missing data in all homogeneous series and sub-series with the same data estimation procedure (Stage 3). All these processes are described in the flow-chart shown in Figure A1. Thresholds for outlier rejection and break-point detection can be very different depending on the data periodicity and cross-correlation of the series. Therefore, it is highly recommended to make a first run in the so-called “exploratory” mode in order to detect these thresholds.

Following the procedure described above, Climatol was applied to our HN dataset. From the exploratory analysis, histograms of maximum windowed and global

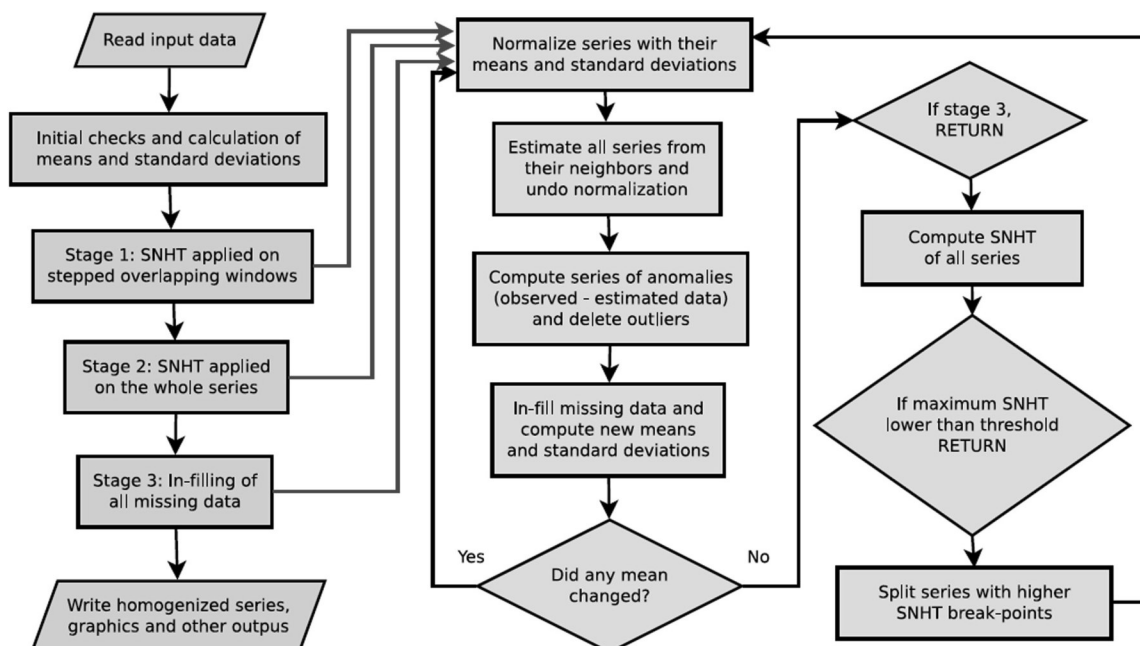
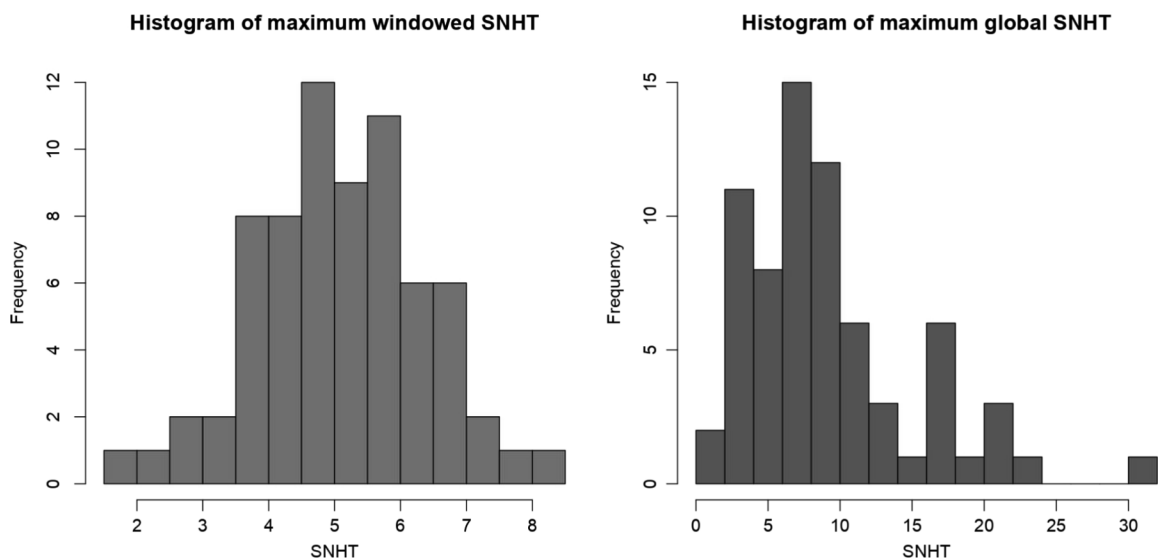
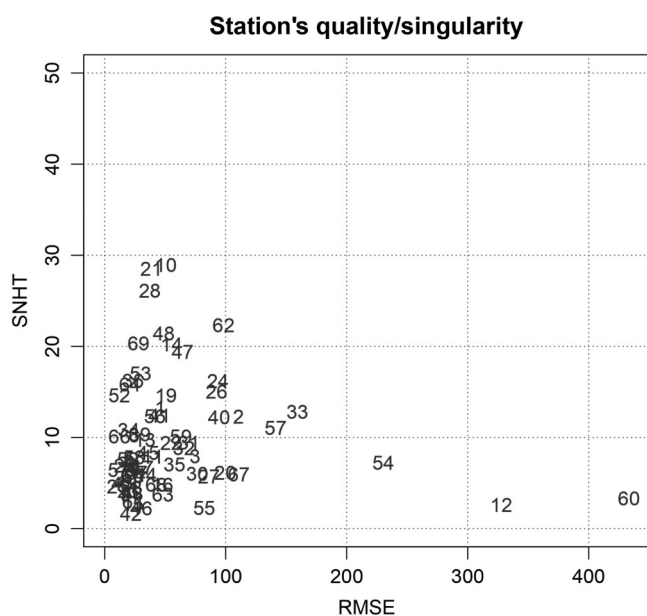


FIGURE A1 Climatol operational flowchart (Guijarro, 2018). [Colour figure can be viewed at wileyonlinelibrary.com]



**FIGURE A2** Histograms of the maximum SNHT values found on overlapping stepped windows (a) and on the whole series (b) using Climatol exploratory mode. [Colour figure can be viewed at [wileyonlinelibrary.com](https://onlinelibrary.wiley.com)]



**FIGURE A3** Distribution of station ID numbers according to their final Root Mean Squared Error (RMSE) and Standard Normal Homogenization Test (SNHT) values evaluated by Climatol. [Colour figure can be viewed at [wileyonlinelibrary.com](https://onlinelibrary.wiley.com)]

SNHT were used to choose the thresholds to detect changes in the mean of the series (Figure A2). These histograms display a prominent occurrence of low values, leading to the conclusion that all the series should be fairly homogeneous. However, considering the histogram of maximum global SNHT, there is one higher and more isolated cluster representing a possible inhomogeneous case. As suggested by Guijarro (2018), when there is a

distinct separation (or a well-defined minimum), the threshold for detection stages can be set to a certain value between them. Therefore, in our case, the threshold value for the stepped SNHT window test applied in stage 1 (snht1) was set to 10, while the threshold value for the SNHT test applied to the complete series in stage 2 (snht2) was set to 30. Moreover, by default, vertical coordinates in meters and horizontal coordinates in kilometres are equally weighted. As done by Buchmann et al. (2022), to consider the impact of elevation, which is a crucial factor for snow, the scale parameter was adjusted to 0.1, so that elevation was given 100 times more weight.

Once the parameters were set, Climatol was run. Figure A3 shows the distribution of station ID numbers (see Table A1) according to their final Root Mean Squared Error (RMSE) and SNHT values. RMSEs are calculated by comparing the estimated and the observed data in every series. High values may indicate poor quality of the series, whereas homogeneous series tend to be clustered in the left bottom part of the plot (Guijarro, 2018). In our case, almost all stations were found to be in the left bottom part of the plot and all stations present SNHT values below the threshold imposed in stage 2 (snht2 = 30), leading to the conclusion that all our series were sufficiently homogeneous. However, there were three of them with a higher RMSE (#54, #12, #60). From Table A1, it can be seen that these stations are those at the highest elevation and consequently those most subjected to errors in HN estimates. For this reason, we decided to not consider these stations for the trend analysis. After a manual quality check, other 21 stations were found to be not suitable for the trend analysis due to the presence of frequent missing data.

APPENDIX C: REGIONALIZATION OVERVIEW

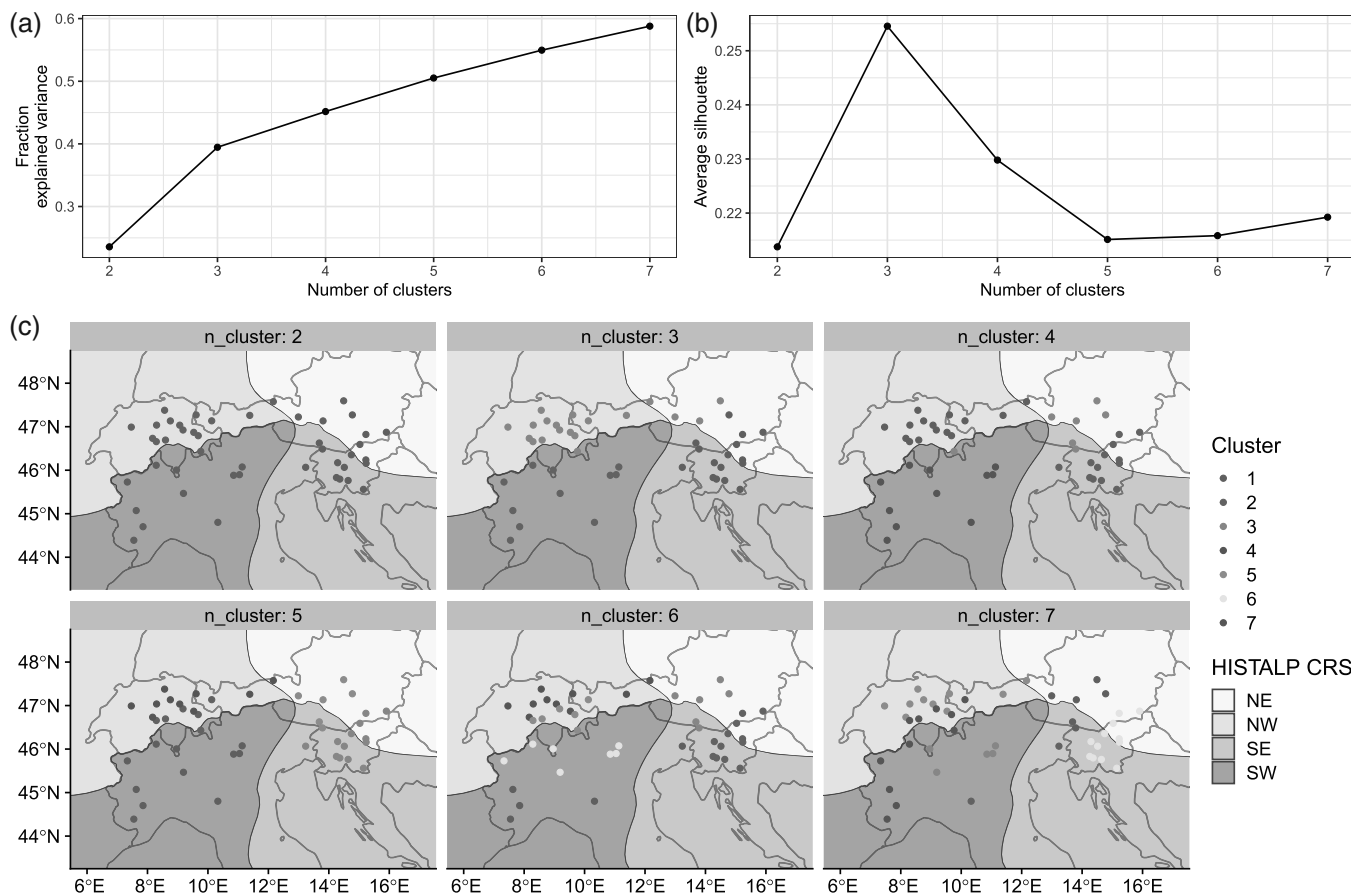


FIGURE A4 Evaluation of k-means clustering results of monthly snowfall (HN) for different numbers of clusters: Ratio of explained variance (a), silhouette (b) and maps (c). [Colour figure can be viewed at wileyonlinelibrary.com]